NASA TECHNICAL MEMORANDUM

NASA TM X-1319

NASA TM X-1319

PROJECT FIRE FLIGHT II AFTERBODY TEMPERATURES AND PRESSURES AT 11.35 KILOMETERS PER SECOND (37 200 FEET PER SECOND)

by Travis H. Slocumb, Jr.

Langley Research Center
Langley Station, Hampton, Va.

NATIONAL AERONAUTICS AND SPACE ADMINISTRATION • WASHINGTON, D. C. • DECEMBER 1966

[redacted] NASA TM X-1319

[redacted]

PROJECT FIRE FLIGHT II AFTERBODY TEMPERATURES AND PRESSURES AT 11.35 KILOMETERS PER SECOND (37 200 FEET PER SECOND)

By Travis H. Slocumb, Jr.

Langley Research Center
Langley Station, Hampton, Va.

[redacted]

[redacted]

[redacted]

[redacted]

NATIONAL AERONAUTICS AND SPACE ADMINISTRATION

[redacted]

PROJECT FIRE FLIGHT II AFTERBODY TEMPERATURES AND PRESSURES AT 11.35 KILOMETERS PER SECOND (37 200 FEET PER SECOND)*

By Travis H. Slocumb, Jr.
Langley Research Center

SUMMARY

The second of two planned Project Fire Flights has been flown to investigate the heating environment on a large-scale, Apollo shape vehicle entering the earth's atmosphere at hyperbolic velocity. The Project Fire flight II spacecraft was boosted into a ballistic trajectory along the Eastern Test Range, with impact occurring near Ascension Island. Prior to reentry into the sensible atmosphere, the reentry vehicle was accelerated to a velocity of 11.35 km/sec (37 200 fps) at a flight-path angle of -14.7° with the local horizon by a solid-propellant rocket motor which formed part of the Fire spacecraft. This report presents the results of heating and pressure experiments on the reentry-vehicle afterbody. A comparison of flight I and flight II afterbody heating and pressure data indicates fair agreement and, in general, both sets of flight data compare favorably with available ground-facility results.

INTRODUCTION

The primary objective of Project Fire was to investigate the heating environment on a blunt-nose vehicle entering the earth's atmosphere at a velocity in excess of escape velocity. The reentry vehicle was instrumented to obtain a measure of radiative heating and total heating on both the forebody and the afterbody as well as limited data on afterbody pressures and telemetry-signal blackout. The first of two planned flights was launched from Cape Kennedy, Florida, on April 14, 1964, and the vehicle successfully reentered the earth's atmosphere near Ascension Island at a velocity of 11.56 km/sec (38 000 fps) and a flight-path angle of -14.7°. The details of the flight I spacecraft, including hardware description, trajectory information, and experimental data, are presented in references 1 to 5. The Project Fire second flight, which was planned as a backup to the first flight, was launched from Cape Kennedy on May 22, 1965. The Fire II payload and flight plan were essentially identical to those of Fire I, and the prime objective of Fire II was to provide verification and extension of Fire I results. The afterbody data obtained on the Fire II reentry package are presented herein.

*Title, Unclassified.

SYMBOLS

D	diameter, centimeters (inches)
h	altitude, kilometers (feet)
l	distance along center line from forward shoulder to theoretical apex of conical afterbody, centimeters (inches) (see fig. 3)
M	Mach number
N_{Re}	Reynolds number (based on maximum diameter of reentry package)
p	pressure, newtons/meter^2 (pounds/inch^2)
$\dot{q}$	heat-transfer rate, watts/centimeter^2 (Btu/foot^2-second)
R	radius, centimeters (inches)
s	surface distance on reentry package measured from geometric stagnation point, centimeters (inches) (see fig. 3)
T	temperature, degrees Kelvin (degrees Rankine)
V	velocity, kilometers/second (feet/second)
x	distance along center line measured from forward shoulder on afterbody, centimeters (inches) (see fig. 3)
γ	isentropic exponent
ϕ	circumferential location, degrees (see fig. 3)

Subscripts:

a	afterbody
av	average

c	corner
calc	calculated
m	pertaining to maximum cross-sectional dimensions
n	nose
sp	sonic point
t	stagnation
∞	free stream

DESCRIPTION OF EXPERIMENT

Space Vehicle

The Project Fire space vehicle was basically an Atlas D launch vehicle coupled with a powered spacecraft as shown in the drawing of figure 1. The powered spacecraft consisted of a velocity package (Antares II-A5 solid rocket motor and adapter shell) together with the reentry package containing the experimental instrumentation. The reentry package and Antares motor were protected from the launch environment by an aerodynamic shroud.

Reentry Package

The Project Fire reentry package was a blunt, Apollo shape vehicle as shown in the photograph of figure 2 and the drawing of figure 3. The forebody consisted of a multilayer configuration made up of three protective phenolic-asbestos shields sandwiched between three beryllium calorimeters. The sequence of events was planned to allow exposure of each beryllium calorimeter until severe melting occurred, and then ejection of the succeeding phenolic-asbestos shield. The first two phenolic-asbestos shields were jettisoned at predetermined deceleration loads to provide beryllium calorimeter measuring periods during the initial part of the heat pulse, at approximately peak heating, and midway on the decreasing side of the heat pulse. The third phenolic-asbestos heat shield was not jettisoned and was provided to protect the reentry package throughout the later stages of reentry should melting of the last calorimeter layer occur. The three beryllium calorimeters were thoroughly instrumented with thermocouples to measure the calorimeter response to the environmental heat flux. Forward-looking radiometers were located at the geometric stagnation point and one offset location to measure the

[redacted]

radiative heating. Details of the forebody experiments and instrumentation on the reentry package are presented in references 3 and 4.

The reentry-package afterbody was conical as shown in the drawing of figure 3 and was constructed of a fiber glass shell to which phenolic-asbestos heat protection material was added. A very thin exterior coating of a protective material (75-percent silicon elastomer and 25-percent high-silica microballoons by weight) was added to prevent moisture penetration prior to launch, thus reducing the possibility of telemetry antenna performance degradation. The afterbody was instrumented with gold-slug calorimeters at 12 locations which provided a measure of the local total heating rates, whereas the total radiative heat flux was measured at 1 location. The only change in the Fire II afterbody instrumentation as compared with that of Fire I was a reduction from two pressure sensors to one, which was located at $x/l = 0.70$. In addition to the other instrumentation, a telemetry antenna was embedded in the afterbody, and a C-band beacon was located at the apex of the conical afterbody for tracking purposes. Table I and the drawing of figure 3 indicate the dimensional location and placement of the afterbody instrumentation. A description of the pressure sensor and the gold calorimeters is given in the following sections.

Pressure sensor.- A thermopile vacuum gage was used to measure the afterbody pressure; it was sized to operate in a range from approximately 13.3 N/m^2 to 1333.2 N/m^2 (0.1 mm Hg to 10 mm Hg). The system accuracy, including that of the sensor and telemetry system, was approximately ±20 percent of the recorded value. The pressure sensor operated continuously, but its output was commutated at five samples per second.

Gold calorimeters.- The gold calorimeters consisted of thin gold slugs mounted as shown in figure 4. The thickness of the gold slugs was approximately 0.305 cm (0.12 in.) to minimize the temperature gradient between the front and rear surfaces. The mass of each calorimeter is presented in table II. An aluminum silicate housing served to insulate the gold slug from the heat of the surrounding materials. In addition, the top surface of each gold slug was coated with a 0.1270-mm-thick (0.005-in.) surface film of oxidized nichrome to increase the emissivity and, consequently, to increase the calorimeter life. A surface-film emissivity of 0.80 was used in the afterbody heating rate calculations. The nichrome oxide surface film was applied to the gold slugs by flame spraying nichrome powder (80-percent nickel, 20-percent chrome) on the surface, vacuum heat treating for 3 hours at 861° K (1550° R), and then allowing oxidation in air for 3 hours at 861° K (1550° R). Two thermocouples were attached to the rear surface of each calorimeter to record the temperature time history during reentry. The diffusion time through the calorimeters was estimated to be less than 1/10 second throughout the reentry, and the measuring accuracy of the thermocouples operating in conjunction with the telemetry system was within ±28° K (±50° R). The gold calorimeter temperatures were commutated at five samples per second.

[redacted]

[redacted] CONFIDENTIAL

TRAJECTORY AND SEQUENCE OF EVENTS

The Fire II space vehicle was launched from Cape Kennedy on May 22, 1965. The flight was along the Atlantic Missile Range with impact of the reentry package occurring in the Atlantic Ocean near Ascension Island. A schematic drawing of the flight trajectory and the associated sequence of events is presented in figure 5. Curves of altitude, velocity, and Mach number are presented in figure 6 for the reentry portion of flight. Details concerning the Fire II trajectory and the atmospheric soundings conducted after the flight are contained in reference 6.

The flight was essentially nominal with all systems operating as planned. The reentry package, spinning about its longitudinal axis at 3 rps, reentered the earth's atmosphere with relatively small body motions. Initially the coning angle was less than 1°, increasing to about 5° just after peak heating and about 11° at the end of the last data-gathering period. These angle-of-attack variations appeared to have very little effect on the measured afterbody data.

RESULTS AND DISCUSSION

Afterbody Pressures

The pressure was measured at one location on the Fire II reentry-package afterbody as shown in figure 3, and these data are listed in table III and plotted in figure 7. The upper portion of figure 7 presents the pressure data in dimensional form as a function of elapsed reentry time from an altitude of 122 km (≈400 000 ft). The data indicate a fairly smooth increasing trend initially; however, above a pressure of approximately 800 N/m^2 (6 mm Hg) the scatter increased markedly. In this region, the readout accuracy was impaired by poor quality data caused by the combination of telemetry noise and sensor inaccuracies as the limit of the thermopile gage was approached. A gap in the pressure data occurred between 28 and 34 seconds because the pressure exceeded the operating limits of the system. After 34 seconds, the pressure decreased to a value again within the range of the pressure sensing system.

In the lower part of figure 7 the Fire II data are plotted in the form of the ratio of afterbody pressure to the calculated stagnation equilibrium pressure behind the shock as a function of the elapsed time from an altitude of 122 km (≈400 000 ft). For comparison purposes, the Fire I data as well as available ground-facility data are superimposed on the figure as a function of free-stream Mach number. The behavior of the Fire II data prior to 22 seconds may be due to the effect of nonequilibrium flow on the front face of the reentry package or flow separation on the afterbody. However, there are insufficient data to substantiate either of these possibilities. The flight I data prior to 20 seconds

[redacted]

exhibit large scatter due to telemetry antenna problems and wide variations caused by large angular fluctuations early in flight (see refs. 2 and 5) and do not correlate well with the flight II data during this time period. However, the Fire I data measured in the later stages of reentry compare favorably with the Fire II data. In addition, comparable ground-facility data (refs. 7, 8, and 9) plotted in this figure exhibit fair agreement with the Project Fire results.

An attempt at correlating the afterbody pressure data with ground-facility data and theoretical calculations is made in figure 8. The data are plotted in the form of p_a/p_∞ as a function of free-stream Mach number. The theoretical curves shown in figure 8 were calculated as outlined in reference 5. In the calculations, the flow was assumed to expand two-dimensionally around the corner from the sonic point to the separation line, which was assumed to be parallel to the free-stream flow. The equilibrium pressure behind the normal shock wave was calculated by using the gas tables of reference 10. The pressure distribution across the front face of the reentry package as well as an estimate of the location of the sonic point on the body surface was determined from flow-field studies on the Fire reentry package (refs. 11, 12, and 13). In addition it was assumed that the location of the sonic point on the small corner radius remained stationary throughout the reentry flight. Data from both Project Fire flights and ground-facility results exhibit fair correlation when plotted in this form. The sudden change in slope in the data at $M_\infty \approx 35$ could be the result of nonequilibrium flow effects or afterbody flow separation, as mentioned previously. Calculations made on the basis of the Fire II trajectory and the tables of references 10 and 14 indicate that very early in flight and in the later stages of reentry, the value of γ_{sp} approached 1.4; however, during the major part of the reentry measuring period, the value of γ_{sp} was approximately 1.2. Thus, the theoretical curves in figure 8 indicate the trends in the afterbody pressure data, but they indicate higher levels of p_a/p_∞ than the measured flight data. A more accurate calculation of the afterbody pressure ratio could be made if the variation in location of the sonic point and the effect of γ_{sp} on the afterbody flow separation line is considered; however, such detailed calculations are beyond the scope of the present report.

Calorimeter Temperatures

The afterbody calorimeter temperatures are presented in table IV and plotted in figure 9 as a function of time from an altitude of 122 km (≈400 000 ft). The temperatures presented are those measured on the rear surfaces of the 12 gold calorimeters located on the reentry-package afterbody as shown in figure 3. The two thermocouples attached to the base of each gold calorimeter (see fig. 4) measured the same temperature within the accuracy of the measuring system; consequently, temperatures from only one thermocouple are presented in this report.

The data shown in figure 9 indicate a general increase in calorimeter temperatures, with small disturbances in the slope of the temperature-time variation occurring near the times of beryllium melt and phenolic-asbestos heat-shield ejections. For reference, the times of these occurrences are noted in figure 9(a). The solid curves in figure 9 represent curve fits of the temperature data which were used in calculating the afterbody heating rates. The scatter in the data is a function of the accuracy of the data-gathering system, whereas the changes in slope of the temperature-time curves are associated with contamination of the afterbody flow field with melted beryllium and heat-shield ablation products.

There was little variation in the temperature data with circumferential location; however, a longitudinal variation was apparent. At a time of 40 seconds, when the maximum calorimeter temperatures were measured, the temperature distribution proceeding rearward along an afterbody element indicates decreasing and then increasing temperatures as the afterbody apex is approached. The maximum temperature of all 12 calorimeters remained less than 670° K (1206° R), an indication that melting of the calorimeter surfaces did not occur during the reentry heat pulse.

Afterbody Heating Rates

The afterbody heating rates were calculated from the temperature variations measured by the 12 gold calorimeters and are presented in figure 10. In general, the heat storage equation combined with curve fits of the smoothed calorimeter temperature-time histories was used in calculating the afterbody heating rates. A description of this method is presented in reference 5. The curve fit of the temperature-time histories for each afterbody calorimeter is presented in figure 9.

The afterbody heating rates are plotted in figure 10 as a function of time from an altitude of 122 km (≈400 000 ft) for the various locations of ϕ and x/l. Throughout reentry the afterbody radiometer indicated zero radiation except for one flash associated with a forebody heat-shield ejection. These data indicate that the afterbody radiation was less than the threshold of intensity of the radiometer, which was approximately 1 W/cm^2 (0.9 Btu/ft^2-sec). It is therefore concluded that the afterbody heating rates consisted mainly of convective heating. Inspection of the curves indicates a rapid initial increase in heating rate with a slow decline after the peak values were reached. In addition, there was a certain amount of scatter in the times at which peak heating rates occurred for all calorimeters, which was associated with the sensitivity in the determination of the inflection points of the temperature-time variation. The maximum heating rates indicated by the calorimeter measurements ranged between 17.8 and 14.5 W/cm^2 (15.7 and 12.8 Btu/ft^2-sec), with the highest values being recorded by the most rearward calorimeters. As was true for the temperature variation, there was no significant circumferential

variation in the heating rate data; however, there did appear to be an effect of longitudinal location. This effect is shown in the summary curve of figure 11.

The ratio of the measured afterbody heating rate to the calculated stagnation convective heating rate is plotted as a function of s/R for the Fire I and Fire II data in figure 11. The stagnation convective heating rates were calculated by using the method of reference 15, and the times for which the Fire I and Fire II data are presented generally correspond to the time of peak afterbody heating. For comparative purposes, afterbody heating data for Apollo shape bodies from various ground facilities (refs. 7 and 9) are plotted in the figure with the respective free-stream flow conditions listed in the key. In general, the Fire I and Fire II data fall within the scatter band of the ground-facility data and favor the high side of the band. The Fire II data exhibit the same type of concave longitudinal distribution with s/R as the ground-facility data. This variation is not present in the Fire I data possibly because of the large body motions that the Fire I reentry package underwent during the reentry portion of flight. For the peak heating conditions, the Fire II afterbody heating rate ratios ranged between 0.038 and 0.044.

CONCLUDING REMARKS

The second of two planned flights has been flown to investigate the heating environment on an Apollo shape vehicle entering the earth's atmosphere at hyperbolic velocity. The reentry package entered the earth's atmosphere at a velocity of 11.35 km/sec (37 200 fps) at a flight-path angle of -14.7° with the local horizon. The vehicle afterbody was instrumented to obtain total and radiative heating rates as well as limited pressure measurements.

The Fire II afterbody pressure data indicate reasonable agreement with the Fire I data and compare favorably with available ground-facility data. Both Fire I and Fire II pressure data correlate well when plotted in the form of the ratio of afterbody pressure to free-stream pressure as a function of free-stream Mach number.

For the range of conditions that the reentry package was exposed to during flight, the afterbody heating rates were mainly composed of convective heating. The maximum heating rate measured on the reentry package afterbody was 17.8 W/cm^2 (15.7 Btu/ft^2-sec) which was measured at the most rearward location on the afterbody. The ratio of the measured afterbody heating rate to the calculated stagnation convective heating rate at

[redacted]

peak heating conditions ranged between 0.038 and 0.044, exhibiting fair agreement with comparable ground-facility results.

Langley Research Center,
National Aeronautics and Space Administration,
Langley Station, Hampton, Va., August 25, 1966,
714-00-00-01-23.

[redacted]

REFERENCES

1. Scallion, William I.; and Lewis, John H., Jr.: Flight Parameters and Vehicle Performance for Project Fire Flight 1, Launched April 14, 1964. NASA TN D-2996, 1965.

2. Woodbury, Gerard E.: Angle-of-Attack Analysis for Project Fire 1 Payload Reentry Flight. NASA TN D-3366, 1966.

3. Cornette, Elden S.: Forebody Temperatures and Total Heating Rates Measured During Project Fire 1 Reentry at 38 000 Feet Per Second. NASA TM X-1120, 1965.

4. Cauchon, Dona L.: Project Fire Flight 1 Radiative Heating Experiment. NASA TM X-1222, 1966.

5. Slocumb, Travis H., Jr.: Project Fire Flight 1 Heating and Pressure Measurements on the Reentry-Vehicle Afterbody at a Velocity of 38 000 Feet Per Second. NASA TM X-1178, 1965.

6. Lewis, John H., Jr.; and Scallion, William I.: Flight Parameters and Vehicle Performance for Project Fire Flight II, Launched May 22, 1965. NASA TN D-3569, 1966.

7. Jones, Robert A.: Experimental Investigation of the Overall Pressure Distribution, Flow Field, and Afterbody Heat-Transfer Distribution of an Apollo Reentry Configuration at a Mach Number of 8. NASA TM X-813, 1963.

8. Gray, J. Don; and Jones, J. H.: Force and Pressure Tests on Apollo Configurations at Mach 1.5 Through 10. AEDC-TDR-63-17, U.S. Air Force, Feb. 1963.

9. Lee, George; and Sundell, Robert E.: Heat-Transfer and Pressure Distributions on Apollo Models at $M = 13.8$ in an Arc-Heated Wind Tunnel. NASA TM X-1069, 1965.

10. Hilsenrath, Joseph; Klein, Max; and Woolley, Harold W.: Tables of Thermodynamic Properties of Air Including Dissociation and Ionization From 1,500° K to 15,000° K. AEDC-TR-59-20, U.S. Air Force, Dec. 1959. (Available from ASTIA as AD229934.)

11. Brunner, M. J.; Dohner, C. V.; Langelo, V. A.; and Rie, H.: Flow Field Prediction and Analysis – Project Fire. Doc. No. 64SD727 (NASA CR-60451), Re-Entry Syst. Dept., Gen. Elec. Co., May 29, 1964.

12. Kuby, W. C.; Byron, S. R.; Foster, R. M.; Hoglund, R. F.; and Holt, M.: Analysis of the Project Fire Re-Entry Package Flow Field. Publ. No. U-3020 (NASA CR-63388), Aeronutronic Div., Philco Corp., Oct. 8, 1964.

13. Vinokur, M.; Nicolet, W. E.; Buckingham, A. C.; and Hoshizaki, H.: Project Fire – Flow Field Prediction and Analysis. M-12-65-1 (NASA CR-63401), Lockheed Missiles & Space Co., Mar. 1965.

14. Hansen, C. Frederick: Approximations for the Thermodynamic and Transport Properties of High-Temperature Air. NASA TR R-50, 1959. (Supersedes NACA TN 4150.)

15. Cohen, Nathaniel B.: Boundary-Layer Similar Solutions and Correlation Equations for Laminar Heat-Transfer Distribution in Equilibrium Air at Velocities up to 41,000 Feet Per Second. NASA TR R-118, 1961.

TABLE I.- AFTERBODY SENSOR LOCATIONS

Station	Afterbody sensors	x/l	$(s/R_m)_{av}$
1	Geometric stagnation point	----	0
2	Heat-shield shoulder	0	1.17
3	3 calorimeters (+) $\phi = 0^o$, 120^o, and 240^o	0.19	1.51
4	1 radiometer (o) $\phi = 203.45^o$	0.32	1.75
5	3 calorimeters (+) $\phi = 0^o$, 120^o, and 240^o	0.38	1.86
6	3 calorimeters (+) $\phi = 0^o$, 120^o, and 240^o	0.56	2.18
7	3 calorimeters (+) $\phi = 0^o$, 120^o, and 240^o 1 pressure sensor (Δ) $\phi = 265^o$	0.70	2.44
8	Theoretical apex of conical afterbody	1.00	2.98

TABLE II.- MASS OF AFTERBODY GOLD CALORIMETERS

Afterbody-calorimeter position		Mass of gold calorimeters, g
ϕ, deg	x/l	
0 ↓	0.19	5.1532
	.38	5.1748
	.56	5.1031
	.70	5.2093
120 ↓	0.19	5.0364
	.38	5.1277
	.56	5.0815
	.70	5.1602
240 ↓	0.19	5.0919
	.38	5.1975
	.56	5.1935
	.70	5.0338

TABLE III.- AFTERBODY PRESSURES MEASURED ON FIRE REENTRY PACKAGE

[$\phi = 265^{\circ}$; $x/l = 0.7$]

Time from altitude of 122 km (≈400 000 ft), sec	Afterbody pressure,		Time from altitude of 122 km (≈400 000 ft), sec	Afterbody pressure,	
	N/m^2	psia		N/m^2	psia
17.00	37.03	0.005	26.60	1303.11	0.189
17.21	56.74	.008	26.81	1027.32	.149
17.41	61.16	.009	27.01	1123.85	.163
17.62	74.46	.011	27.21	1303.11	.189
17.82	96.53	.014	27.62	820.48	.119
18.06	106.18	.015	34.58	1303.11	.189
18.23	85.50	.012	34.78	1123.85	.163
18.44	89.63	.013	35.19	1123.85	.163
18.65	128.93	.019	35.39	1303.11	.189
18.85	143.41	.021	35.79	1303.11	.189
19.06	183.40	.027	36.00	1123.85	.163
19.26	211.67	.031	36.20	1303.11	.189
19.47	230.97	.034	36.40	1027.32	.149
19.67	243.39	.035	36.80	1303.11	.189
19.88	253.04	.037	37.20	1303.11	.189
20.08	297.16	.043	37.40	1303.11	.189
20.29	351.63	.051	37.61	1123.85	.163
20.49	393.00	.057	37.81	1123.85	.163
20.69	445.40	.065	38.01	1303.11	.189
20.90	393.00	.057	38.40	1123.85	.163
21.10	546.07	.079	38.61	1303.11	.189
21.30	639.14	.093	38.80	1027.32	.149
21.51	639.14	.093	39.01	820.48	.119
21.71	689.48	.100	39.20	910.11	.132
21.91	593.64	.086	39.40	820.48	.119
22.12	689.48	.100	39.60	1123.85	.163
22.32	820.48	.119	39.80	910.11	.132
22.52	820.48	.119	40.00	758.42	.110
22.93	1303.11	.189	40.20	820.48	.119
23.34	1303.11	.189	40.40	758.42	.110
23.54	1123.85	.163	40.60	689.48	.110
23.75	1303.11	.189	40.80	758.42	.110
23.95	1303.11	.189	40.99	689.48	.100
24.16	1027.32	.149	41.19	820.48	.119
24.36	1027.32	.149	41.39	639.14	.093
24.56	820.48	.119	41.59	828.48	.119
24.76	-------	-----	41.79	445.40	.065
24.97	1027.32	.149	41.99	689.48	.100
25.17	1123.85	.163	42.19	758.42	.110
25.38	1123.85	.163	42.39	758.42	.110
25.58	1123.85	.163	42.59	689.48	.100
25.78	1027.32	.149	42.79	689.48	.100
25.99	1027.32	.149	42.99	758.42	.110
26.19	1303.11	.189	43.18	504.01	.073
26.40	1027.32	.149	43.38	758.42	.110

TABLE IV.- AFTERBODY TEMPERATURES MEASURED ON PROJECT FIRE REENTRY PACKAGE

Afterbody temperatures, ^{o}K											
$\phi = 0^{o}$								$\phi = 120^{o}$			
Time from 122 km (400 000 ft) sec	$\frac{x}{l} = .19$	Time from 122 km (400 000 ft) sec	$\frac{x}{l} = .38$	Time from 122 km (400 000 ft) sec	$\frac{x}{l} = .56$	Time from 122 km (400 000 ft) sec	$\frac{x}{l} = .70$	Time from 122 km (400 000 ft) sec	$\frac{x}{l} = .19$	Time from 122 km (400 000 ft) sec	$\frac{x}{l} = .38$
16.14	319.85	16.15	310.04	16.17	307.90	16.18	311.10	16.20	311.10	16.21	310.57
16.33	303.10	16.34	299.88	16.36	302.56	16.37	302.56	16.39	301.49	16.40	301.49
16.52	319.34	16.54	306.83	16.55	306.83	16.57	311.11	16.58	314.20	16.60	309.51
16.72	306.87	16.73	309.55	16.75	307.40	16.76	307.94	16.78	306.33	16.79	311.16
16.91	301.50	16.92	301.50	16.94	301.50	16.95	301.50	16.97	301.50	16.98	297.19
17.10	316.32	17.12	312.18	17.13	307.93	17.15	305.25	17.16	309.54	17.18	311.15
17.30	304.75	17.31	306.37	17.33	306.91	17.34	306.37	17.36	303.13	17.37	303.67
17.49	312.26	17.50	307.45	17.52	307.45	17.53	307.45	17.55	309.07	17.56	305.29
17.68	321.52	17.70	313.76	17.71	314.28	17.73	317.38	17.74	312.72	17.76	315.31
17.88	324.65	17.89	317.40	17.91	323.09	17.92	322.06	17.94	322.06	17.95	317.91
18.07	324.12	18.08	317.91	18.10	317.91	18.11	311.69	18.13	312.73	18.14	314.80
18.26	330.85	18.28	323.60	18.29	323.60	18.31	323.60	18.32	332.92	18.34	322.05
18.46	340.09	18.47	329.24	18.49	332.85	18.50	334.92	18.52	338.54	18.53	331.82
18.65	327.79	18.66	314.82	18.68	326.24	18.69	325.20	18.71	328.31	18.72	330.39
18.84	334.20	18.86	321.68	18.87	325.85	18.89	326.38	18.90	330.55	18.92	321.16
19.04	344.38	19.05	339.71	19.07	345.41	19.08	334.52	19.10	338.67	19.11	329.34
19.23	344.05	19.24	333.11	19.26	340.93	19.27	348.74	19.29	348.74	19.30	344.05
19.42	367.41	19.44	353.48	19.45	355.02	19.47	356.06	19.48	359.67	19.50	348.31
19.62	367.53	19.63	353.57	19.65	358.22	19.66	359.26	19.68	361.33	19.69	353.57
19.81	379.84	19.82	379.84	19.84	371.06	19.85	364.35	19.87	368.99	19.88	359.70
20.03	374.03	20.02	355.98	20.03	375.06	20.05	370.42	20.06	367.33	20.08	360.11
20.23	365.32	20.21	360.68	20.23	365.32	20.24	364.80	20.26	375.64	20.27	364.29
20.39	378.57	20.40	368.27	20.42	374.45	20.43	367.75	20.45	375.99	20.46	368.27
20.58	376.91	20.60	363.97	20.61	363.45	20.63	365.52	20.64	366.56	20.66	361.90
20.78	375.30	20.79	359.15	20.81	368.01	20.82	368.01	20.84	374.78	20.85	368.01
20.97	389.28	20.98	371.48	21.00	377.24	21.01	377.24	21.03	385.09	21.04	363.63
21.16	379.86	21.18	364.68	21.19	364.68	21.21	367.29	21.22	376.72	21.24	365.20
21.36	394.24	21.37	369.05	21.39	374.30	21.40	374.82	21.42	383.22	21.43	372.20
21.55	384.79	21.56	364.32	21.58	371.67	21.59	371.67	21.61	378.49	21.62	374.30
21.74	392.93	21.76	383.56	21.77	389.29	21.79	389.29	21.80	395.01	21.82	382.00
21.94	411.34	21.95	396.92	21.97	392.24	21.98	395.88	22.00	400.65	22.01	387.57
22.13	402.35	22.15	389.21	22.16	400.75	22.17	391.29	22.19	395.45	22.20	391.29
22.32	408.72	22.34	390.73	22.35	401.77	22.37	396.96	22.38	409.26	22.40	396.44
22.52	409.16	22.53	393.17	22.55	401.11	22.56	401.11	22.58	402.19	22.59	394.22
22.71	406.14	22.73	390.20	22.74	398.61	22.75	398.61	22.77	398.61	22.78	398.61
22.90	435.98	22.92	404.62	22.93	407.21	22.95	410.94	22.96	419.46	22.98	405.62
23.10	420.32	23.11	403.77	23.13	411.78	23.14	411.78	23.16	417.65	23.17	406.97
23.29	430.59	23.31	408.14	23.32	417.22	23.34	422.03	23.35	426.31	23.36	413.48
23.48	427.74	23.50	413.86	23.51	414.40	23.53	420.80	23.54	411.73	23.56	413.33
23.68	424.96	23.69	386.86	23.71	417.49	23.72	417.49	23.74	414.29	23.75	408.43
23.87	429.75	23.89	413.69	23.90	416.90	23.92	417.97	23.93	431.89	23.94	416.36
24.06	437.45	24.08	414.04	24.09	425.21	24.11	423.61	24.12	424.68	24.14	416.70
24.26	439.80	24.27	412.51	24.29	425.35	24.30	429.63	24.32	434.98	24.33	413.58
24.45	438.32	24.47	416.36	24.48	423.33	24.50	432.96	24.51	431.89	24.53	420.11
24.64	447.24	24.66	423.96	24.67	437.18	24.69	435.07	24.70	437.71	24.72	435.07
24.84	453.33	24.85	433.19	24.87	433.72	24.88	441.67	24.90	443.79	24.91	431.60
25.03	455.64	25.05	431.60	25.06	431.06	25.08	436.40	25.09	436.40	25.11	425.18
25.22	462.10	25.24	446.17	25.25	445.11	25.27	448.29	25.28	445.64	25.30	436.61
25.42	457.60	25.43	440.58	25.45	440.05	25.46	448.56	25.48	437.92	25.49	437.92
25.61	461.12	25.63	437.60	25.64	442.94	25.66	449.89	25.67	452.57	25.69	446.69
25.80	463.63	25.82	442.19	25.83	447.55	25.85	453.98	25.86	455.59	25.88	441.66
				26.03	433.75	26.04	441.82	26.06	439.67	26.07	440.75

TABLE IV.- AFTERBODY TEMPERATURES MEASURED ON PROJECT FIRE REENTRY PACKAGE - Continued

Afterbody temperatures, ^{o}K											
$\phi = 0^{o}$								$\phi = 120^{o}$			
Time from 122 km (400 000 ft) sec	$\frac{x}{l} = .19$	Time from 122 km (400 000 ft) sec	$\frac{x}{l} = .38$	Time from 122 km (400 000 ft) sec	$\frac{x}{l} = .56$	Time from 122 km (400 000 ft) sec	$\frac{x}{l} = .70$	Time from 122 km (400 000 ft) sec	$\frac{x}{l} = .19$	Time from 122 km (400 000 ft) sec	$\frac{x}{l} = .38$
26.00	459.60	26.01	431.59	26.22	444.37	26.24	451.93	26.25	456.25	26.27	442.21
26.19	463.27	26.21	444.37	26.41	454.50	26.43	463.58	26.44	453.43	26.46	453.43
26.38	469.45	26.40	451.29	26.61	456.73	26.62	443.33	26.64	451.91	26.65	471.21
26.58	484.59	26.59	483.54	27.02	457.07	27.04	468.77	27.05	465.05	27.07	457.60
26.99	475.68	27.01	459.73	27.22	455.78	27.24	469.68	27.25	465.40	27.27	456.85
27.19	476.10	27.21	455.78	27.42	453.50	27.43	462.05	27.45	464.18	27.46	451.36
27.39	477.54	27.40	458.31	27.62	444.35	27.63	458.24	27.65	461.97	27.66	451.29
27.59	465.18	27.60	448.62	27.81	465.45	27.83	477.10	27.85	473.39	27.86	466.51
27.78	487.10	27.80	468.62	28.01	464.09	28.03	478.90	28.04	468.85	28.06	463.04
27.98	479.43	28.00	460.92	28.21	465.80	28.23	484.42	28.24	478.58	28.26	466.33
28.18	486.52	28.20	468.46	28.41	467.97	28.42	484.19	28.44	483.12	28.45	467.43
28.38	493.76	28.39	464.72	28.61	477.03	28.62	491.00	28.64	481.37	28.65	469.98
28.58	506.98	28.59	478.12	28.80	470.37	28.82	489.23	28.84	459.53	28.85	467.12
28.77	493.49	28.79	469.28	29.00	486.48	29.02	501.17	29.03	495.40	29.05	482.27
28.97	497.50	28.99	479.60	29.20	480.55	29.22	504.47	29.23	496.51	29.25	485.37
29.17	498.10	29.19	483.25	29.40	484.72	29.41	505.46	29.43	489.51	29.44	485.79
29.37	504.93	29.38	477.71	29.60	486.57	29.61	508.93	29.63	491.89	29.64	480.12
29.57	502.54	29.58	477.41	29.80	485.99	29.81	502.44	29.83	489.70	29.84	477.93
29.76	505.62	29.78	478.47	29.99	499.77	30.01	523.86	30.02	512.34	30.04	495.58
29.96	521.24	29.98	496.63	30.19	497.42	30.21	520.43	30.22	512.06	30.24	494.80
30.16	516.77	30.18	491.14	30.39	484.02	30.40	519.20	30.42	506.60	30.44	492.95
30.36	508.18	30.37	465.86	30.59	499.60	30.60	530.64	30.62	508.54	30.63	496.97
30.56	525.90	30.57	490.66	30.79	494.33	30.80	521.75	30.82	503.82	30.83	485.89
30.76	524.92	30.77	491.16	30.98	498.99	31.00	522.97	31.01	513.38	31.03	497.92
30.95	523.50	30.97	498.99	31.18	502.94	31.20	536.63	31.21	521.89	31.23	503.46
31.15	530.31	31.17	502.41	31.38	510.40	31.40	536.93	31.41	519.95	31.43	504.56
31.35	530.57	31.36	502.44	31.58	506.13	31.59	540.54	31.61	527.83	31.62	507.72
31.55	530.48	31.56	506.13	31.78	511.12	31.79	535.02	31.81	515.90	31.82	510.59
31.75	528.65	31.76	505.81	31.97	507.65	31.99	542.13	32.00	522.51	32.02	503.41
31.94	535.24	31.96	507.65	32.17	509.74	32.19	536.93	32.20	518.80	32.22	490.55
32.14	534.26	32.16	501.21	32.37	523.40	32.39	570.14	32.40	539.68	32.42	523.93
32.34	548.61	32.36	513.43	32.57	528.55	32.58	563.72	32.60	545.87	32.61	528.03
32.54	549.02	32.55	523.31	32.77	526.23	32.78	565.12	32.80	550.40	32.81	529.38
32.74	553.56	32.75	527.80	32.96	532.74	32.98	570.61	32.99	545.89	33.01	528.01
32.93	551.68	32.95	530.64	33.16	533.58	33.18	568.34	33.19	546.74	33.21	530.41
33.13	558.33	33.15	523.57	33.36	530.62	33.38	565.94	33.39	544.85	33.41	524.29
33.33	549.07	33.35	527.98	33.56	551.09	33.57	576.76	33.59	553.71	33.60	541.14
33.53	570.99	33.54	540.10	33.76	550.49	33.77	585.80	33.79	563.50	33.80	547.89
33.73	580.15	33.74	539.05	33.95	546.45	33.97	589.59	33.99	562.62	34.00	544.89
33.92	573.58	33.94	545.41	34.15	547.93	34.17	589.06	34.18	561.52	34.20	546.89
34.12	575.63	34.14	542.71	34.35	546.90	34.37	585.60	34.38	560.00	34.40	547.43
34.32	574.14	34.34	535.91	34.55	547.38	34.56	592.46	34.58	557.92	34.59	546.33
34.52	572.67	34.53	541.58	34.75	540.94	34.76	591.70	34.78	558.81	34.79	543.05
34.72	570.37	34.73	539.89	34.95	538.85	34.96	586.69	34.98	553.76	34.99	540.98
34.91	567.61	34.93	530.33	35.14	542.80	35.16	590.18	35.17	548.14	35.19	533.72
35.11	557.23	35.13	533.18	35.34	527.36	35.36	586.35	35.37	554.21	35.39	541.32
35.31	565.48	35.33	541.86	35.54	536.91	35.55	589.06	35.57	550.39	35.59	533.68
35.51	569.26	35.52	535.83	35.74	531.58	35.75	587.41	35.77	541.35	35.78	524.52
35.71	556.56	35.72	521.26	35.94	561.45	35.95	600.90	35.97	568.78	35.98	554.12
35.91	588.54	35.92	554.65	36.13	565.35	36.15	611.62	36.16	574.33	36.18	556.38
36.10	596.69	36.12	551.62	36.33	570.06	36.35	610.61	36.36	563.71	36.38	563.71
				36.53	557.42	36.55	606.43	36.56	569.15	36.58	552.61

TABLE IV.- AFTERBODY TEMPERATURES MEASURED ON PROJECT FIRE REENTRY PACKAGE - Continued

Afterbody temperatures, ^{o}K											
$\phi = 0^{o}$								$\phi = 120^{o}$			
Time from 122 km (400 000 ft) sec	$\frac{x}{l} = .19$	Time from 122 km (400 000 ft) sec	$\frac{x}{l} = .38$	Time from 122 km (400 000 ft) sec	$\frac{x}{l} = .56$	Time from 122 km (400 000 ft) sec	$\frac{x}{l} = .70$	Time from 122 km (400 000 ft) sec	$\frac{x}{l} = .19$	Time from 122 km (400 000 ft) sec	$\frac{x}{l} = .38$
36.30	585.86	36.32	558.42	36.73	560.60	36.74	609.21	36.76	572.92	36.77	557.39
36.50	591.87	36.51	549.95	36.93	557.27	36.94	606.47	36.96	564.23	36.97	554.06
36.70	594.59	36.71	552.36	37.12	577.33	37.14	629.23	37.15	576.80	37.17	563.66
36.90	590.81	36.91	551.92	37.32	577.87	37.34	626.97	37.35	582.63	37.37	587.80
37.09	598.49	37.11	565.24	37.52	574.66	37.54	624.16	37.55	580.45	37.57	566.76
37.29	601.72	37.31	570.47	37.72	583.06	37.73	620.09	37.75	583.06	37.76	568.29
37.49	604.14	37.50	566.23	37.92	581.29	37.93	632.53	37.95	584.92	37.96	568.15
37.69	605.18	37.70	567.23	38.11	581.69	38.13	618.06	38.14	582.21	38.16	570.66
37.89	613.08	37.90	571.83	38.31	583.44	38.33	625.27	38.34	579.25	38.36	569.31
38.08	611.41	38.10	574.86	38.51	580.67	38.53	628.60	38.54	590.52	38.56	574.33
38.28	610.47	38.30	572.97	38.71	579.96	38.72	628.21	38.74	584.14	38.75	568.39
38.48	611.10	38.50	578.56	38.91	583.73	38.92	631.49	38.94	585.27	38.95	570.04
38.68	609.76	38.69	574.70	39.10	579.77	39.12	625.61	39.14	582.93	39.15	572.39
38.88	613.00	38.89	577.94	39.30	579.27	39.32	626.93	39.33	585.57	39.35	569.72
39.07	613.27	39.09	572.39	39.50	582.49	39.52	633.13	39.53	587.11	39.55	570.95
39.27	616.59	39.29	576.48	39.70	575.88	39.71	630.01	39.73	584.37	39.74	572.69
39.47	612.67	39.49	578.82	39.90	572.92	39.91	624.35	39.93	579.89	39.94	560.06
39.67	605.63	39.68	575.88	40.10	569.95	40.11	621.50	40.13	572.63	40.14	557.62
39.87	601.38	39.88	572.92	40.29	563.20	40.31	620.14	40.32	565.91	40.34	549.13
40.06	607.39	40.08	561.91	40.49	557.18	40.51	611.20	40.52	565.31	40.54	551.76
40.26	599.57	40.28	563.20	40.69	576.79	40.70	631.47	40.72	586.64	40.74	569.47
40.46	592.18	40.48	551.76	40.89	581.86	40.90	628.59	40.92	590.20	40.93	563.76
40.66	612.11	40.67	582.54	41.09	579.38	41.10	630.56	41.12	583.13	41.13	564.95
40.86	626.00	40.87	570.15	41.28	576.31	41.30	632.08	41.31	582.77	41.33	565.54
41.06	605.02	41.07	575.64	41.48	565.42	41.50	615.48	41.51	573.46	41.53	551.49
41.25	608.48	41.27	572.00	41.68	568.13	41.70	610.10	41.71	572.99	41.73	552.46
41.45	609.73	41.47	564.35	41.88	551.88	41.89	627.43	41.91	585.78	41.92	575.42
41.65	599.57	41.66	561.11	42.08	590.71	42.09	638.09	42.11	598.87	42.12	579.41
41.85	626.92	41.86	589.34	42.27	590.82	42.29	645.03	42.30	601.05	42.32	579.46
42.05	619.24	42.06	590.71	42.47	577.98	42.49	636.55	42.50	597.59	42.52	579.56
42.24	618.44	42.26	590.82	42.67	585.66	42.69	639.56	42.70	590.28	42.72	574.66
42.44	619.64	42.46	588.37	42.87	576.61	42.88	630.06	42.90	594.50	42.91	569.41
42.64	612.86	42.65	585.66	43.07	583.36	43.08	627.98	43.10	599.77	43.11	574.94
42.84	622.33	42.85	582.63	43.26	583.39	43.28	631.51	43.29	595.16	43.31	570.78
43.04	613.11	43.05	583.36	43.46	568.98	43.48	630.46	43.49	586.30	43.51	569.51
43.23	608.98	43.25	574.46	43.66	583.06	43.68	627.29	43.69	596.44	43.71	565.65
43.43	613.51	43.45	582.68								
43.63	608.26	43.65	583.06								

TABLE IV.- AFTERBODY TEMPERATURES MEASURED ON PROJECT FIRE REENTRY PACKAGE - Continued

Afterbody temperatures, ^{o}K											
$\phi = 120^{o}$				$\phi = 240^{o}$							
Time from 122 km (400 000 ft) sec	$\frac{x}{l} = .56$	Time from 122 km (400 000 ft) sec	$\frac{x}{l} = .70$	Time from 122 km (400 000 ft) sec	$\frac{x}{l} = .19$	Time from 122 km (400 000 ft) sec	$\frac{x}{l} = .38$	Time from 122 km (400 000 ft) sec	$\frac{x}{l} = .56$	Time from 122 km (400 000 ft) sec	$\frac{x}{l} = .70$
16.22	312.13	16.24	311.10	16.08	320.36	16.09	312.65	16.11	320.88	16.12	313.16
16.42	304.71	16.43	306.85	16.27	316.30	16.28	312.17	16.30	312.68	16.31	307.92
16.61	312.14	16.63	312.14	16.46	329.12	16.48	323.46	16.49	323.46	16.51	319.34
16.80	309.01	16.82	311.16	16.66	317.37	16.67	322.54	16.69	317.37	16.70	311.68
17.00	298.26	17.01	307.43	16.85	304.73	16.86	307.97	16.88	305.81	16.89	301.50
17.19	308.47	17.21	306.86	17.04	320.97	17.06	320.97	17.07	312.70	17.09	318.90
17.39	306.91	17.40	309.08	17.24	317.48	17.25	317.48	17.27	315.92	17.28	313.31
17.58	315.83	17.59	310.15	17.43	320.58	17.44	315.38	17.46	320.58	17.47	316.42
17.77	312.20	17.79	317.90	17.62	327.22	17.64	325.15	17.65	328.25	17.67	330.32
17.97	320.50	17.98	324.65	17.82	326.72	17.83	329.31	17.85	325.17	17.86	323.61
18.16	313.76	18.17	319.46	18.01	323.60	18.02	323.60	18.04	321.01	18.05	324.12
18.35	327.23	18.37	333.96	18.20	339.14	18.22	336.55	18.23	336.03	18.25	339.14
18.55	332.34	18.56	330.27	18.40	344.74	18.41	344.74	18.43	340.09	18.44	343.70
18.74	334.54	18.75	341.80	18.59	330.39	18.60	332.46	18.62	330.91	18.63	336.09
18.93	325.85	18.95	299.88	18.78	342.02	18.80	332.63	18.81	323.25	18.83	334.20
19.13	328.30	19.14	347.49	18.98	349.04	18.99	349.04	19.01	344.89	19.02	345.93
19.32	346.13	19.33	350.82	19.17	350.82	19.18	338.32	19.20	344.05	19.21	347.70
19.51	356.06	19.53	364.32	19.36	362.77	19.38	360.19	19.39	363.28	19.41	370.51
19.71	358.74	19.72	359.26	19.56	370.12	19.57	361.33	19.59	367.02	19.60	369.60
19.90	364.86	19.91	374.68	19.75	374.68	19.77	368.99	19.78	371.06	19.79	380.87
20.09	366.30	20.11	379.19	19.94	372.48	19.96	368.36	19.97	368.36	19.99	376.09
20.29	364.29	20.30	381.83	20.14	380.80	20.15	365.32	20.17	371.00	20.18	377.19
20.48	374.96	20.49	380.63	20.33	387.32	20.35	374.96	20.36	379.08	20.37	382.69
20.67	366.04	20.69	378.98	20.52	376.91	20.54	368.63	20.55	368.63	20.57	385.19
20.87	379.47	20.88	387.28	20.72	375.82	20.73	366.45	20.75	366.45	20.76	380.51
21.06	372.53	21.07	389.80	20.91	387.18	20.93	373.05	20.94	378.81	20.96	389.28
21.25	371.48	21.27	382.47	21.10	378.29	21.12	374.10	21.13	377.24	21.15	399.82
21.45	375.35	21.46	383.22	21.30	378.49	21.31	370.62	21.33	377.97	21.34	390.04
21.64	374.30	21.65	381.12	21.49	388.47	21.51	377.97	21.52	377.97	21.54	384.79
21.83	390.85	21.85	402.44	21.68	406.19	21.70	396.57	21.71	393.45	21.73	393.45
22.03	392.76	22.04	403.86	21.88	408.14	21.89	396.92	21.91	400.65	21.92	409.21
22.22	393.37	22.23	405.63	22.07	407.16	22.09	393.89	22.10	398.61	22.12	407.70
22.41	403.91	22.43	415.14	22.26	398.56	22.28	398.56	22.29	398.03	22.31	417.28
22.61	404.87	22.62	411.85	22.46	412.92	22.47	403.80	22.49	403.80	22.50	409.16
22.80	414.52	22.81	417.43	22.65	410.44	22.67	403.45	22.68	403.45	22.70	420.12
22.99	412.01	23.01	424.79	22.84	426.92	22.86	416.27	22.87	416.27	22.89	425.86
23.19	411.24	23.20	424.06	23.04	425.13	23.05	410.71	23.07	414.45	23.08	429.40
23.38	420.43	23.39	434.86	23.23	422.03	23.25	422.03	23.26	417.76	23.28	432.72
23.57	416.00	23.59	424.00	23.42	429.88	23.44	425.07	23.45	421.33	23.47	433.08
23.77	413.23	23.78	432.96	23.62	427.63	23.63	420.16	23.65	414.29	23.66	430.29
23.96	421.18	23.97	435.10	23.81	436.18	23.83	420.11	23.84	424.93	23.86	438.32
24.15	423.61	24.17	431.06	24.00	438.51	24.02	423.61	24.03	430.00	24.05	441.17
24.35	430.70	24.36	439.26	24.20	430.70	24.21	424.28	24.23	429.63	24.24	447.82
24.54	423.86	24.55	438.85	24.39	441.53	24.41	425.47	24.42	428.14	24.44	438.85
24.73	436.65	24.75	459.41	24.58	448.29	24.60	437.71	24.61	440.36	24.63	458.35
24.93	441.14	24.94	449.09	24.78	451.21	24.79	441.14	24.81	441.14	24.82	463.93
25.12	431.06	25.13	448.16	24.97	450.83	24.99	438.54	25.00	434.80	25.02	452.43
25.31	445.11	25.33	454.13	25.16	448.29	25.18	452.54	25.19	455.73	25.21	470.06
25.51	443.77	25.52	464.52	25.36	451.75	25.37	449.62	25.39	449.09	25.40	470.37
25.70	449.36	25.72	462.19	25.55	450.43	25.57	445.08	25.58	440.80	25.60	464.87
25.89	450.77	25.91	459.34	25.74	451.84	25.76	451.84	25.77	449.70	25.79	471.13
26.09	442.90	26.10	464.98								

TABLE IV.- AFTERBODY TEMPERATURES MEASURED ON PROJECT FIRE REENTRY PACKAGE - Continued

Afterbody temperatures, ^{o}K											
$\phi = 120^{o}$				$\phi = 240^{o}$							
Time from 122 km (400 000 ft) sec	$\frac{x}{l} = .56$	Time from 122 km (400 000 ft) sec	$\frac{x}{l} = .70$	Time from 122 km (400 000 ft) sec	$\frac{x}{l} = .19$	Time from 122 km (400 000 ft) sec	$\frac{x}{l} = .38$	Time from 122 km (400 000 ft) sec	$\frac{x}{l} = .56$	Time from 122 km (400 000 ft) sec	$\frac{x}{l} = .70$
26.28	446.53	26.30	459.49	25.94	456.90	25.95	447.21	25.97	448.83	25.98	468.21
26.47	458.24	26.49	470.52	26.13	469.75	26.15	456.79	26.16	456.79	26.18	479.47
26.67	470.14	26.68	446.61	26.32	471.59	26.34	458.24	26.35	463.58	26.37	486.48
27.08	458.13	27.10	470.90	26.52	465.31	26.53	455.66	26.55	470.14	26.56	493.54
27.28	463.26	27.30	471.82	26.71	474.62	26.73	468.77	26.74	463.45	26.76	492.54
27.48	458.84	27.49	472.20	27.13	470.75	27.14	460.05	27.16	464.33	27.17	483.05
27.68	457.17	27.69	483.34	27.33	470.60	27.34	464.18	27.36	464.18	27.37	490.24
27.88	472.33	27.89	482.93	27.53	466.78	27.54	459.84	27.56	459.84	27.57	487.53
28.07	464.09	28.09	486.78	27.72	479.75	27.74	477.63	27.75	476.57	27.77	504.80
28.27	467.93	28.29	496.46	27.92	473.09	27.94	468.33	27.95	470.97	27.97	493.01
28.47	481.50	28.48	493.76	28.12	485.47	28.13	482.31	28.15	476.99	28.17	504.31
28.67	475.40	28.68	494.73	28.32	486.85	28.33	480.96	28.35	486.32	28.36	506.52
28.87	468.20	28.88	494.55	28.52	491.53	28.53	487.80	28.55	487.80	28.56	510.71
29.06	492.25	29.08	509.57	28.71	502.01	28.73	492.96	28.74	486.57	28.76	507.33
29.26	492.80	29.28	510.31	28.91	510.62	28.93	494.88	28.94	490.68	28.96	512.71
29.46	488.98	29.48	513.96	29.11	512.96	29.12	499.17	29.14	492.80	29.16	520.92
29.66	497.75	29.67	516.38	29.31	515.56	29.32	500.67	29.34	497.48	29.35	515.03
29.86	489.17	29.87	507.75	29.51	515.85	29.52	497.21	29.54	497.21	29.55	533.95
30.05	509.72	30.07	530.15	29.70	511.99	29.72	499.25	29.73	498.19	29.75	530.04
30.25	508.40	30.27	528.27	29.90	532.76	29.92	517.58	29.93	515.48	29.95	548.48
30.45	515.53	30.47	532.33	30.10	536.12	30.12	522.00	30.13	519.38	30.15	544.49
30.65	513.12	30.66	532.21	30.30	529.18	30.31	513.95	30.33	505.55	30.34	531.80
30.85	485.89	30.86	512.79	30.50	537.47	30.51	520.64	30.53	510.65	30.54	547.99
31.04	511.78	31.06	529.36	30.69	529.14	30.71	519.64	30.72	509.10	30.74	546.54
31.24	517.68	31.26	536.10	30.89	535.22	30.91	523.50	30.92	512.31	30.94	552.81
31.44	519.95	31.46	547.02	31.09	537.16	31.11	527.68	31.12	516.10	31.14	560.32
31.64	523.60	31.65	546.36	31.29	542.77	31.30	530.04	31.32	519.42	31.33	561.35
31.84	521.21	31.85	544.58	31.49	549.01	31.50	532.07	31.52	518.84	31.53	563.83
32.04	519.85	32.05	543.20	31.68	540.86	31.70	525.46	31.72	519.09	31.73	560.52
32.23	499.08	32.25	509.74	31.88	541.07	31.90	528.34	31.91	528.34	31.93	563.35
32.43	537.06	32.45	573.81	32.08	543.33	32.10	534.80	32.11	518.27	32.13	562.52
32.63	532.75	32.64	571.59	32.28	558.58	32.29	537.58	32.31	537.58	32.32	599.64
32.83	543.57	32.84	578.26	32.48	560.57	32.49	551.12	32.51	536.43	32.52	585.19
33.03	540.10	33.04	575.87	32.68	564.07	32.69	550.40	32.71	549.35	32.72	585.04
33.22	543.58	33.24	577.82	32.87	562.20	32.89	545.36	32.90	545.36	32.92	591.44
33.42	542.22	33.44	572.27	33.07	556.75	33.09	555.70	33.10	545.16	33.12	600.03
33.62	556.85	33.63	590.19	33.27	563.83	33.28	551.71	33.30	540.11	33.31	590.02
33.82	560.90	33.83	597.46	33.47	575.18	33.48	569.42	33.50	557.38	33.51	604.48
34.02	556.89	34.03	595.69	33.67	580.67	33.68	570.78	33.70	560.90	33.71	609.63
34.21	563.61	34.23	600.77	33.86	576.71	33.88	554.80	33.89	560.54	33.91	610.94
34.41	551.62	34.43	599.38	34.06	587.03	34.08	565.18	34.09	547.93	34.11	614.52
34.61	555.28	34.63	594.51	34.26	571.52	34.27	560.52	34.29	560.52	34.31	614.69
34.81	558.81	34.82	596.31	34.46	572.15	34.47	556.86	34.49	553.70	34.50	615.57
35.01	554.83	35.02	596.04	34.66	580.36	34.67	563.02	34.69	554.61	34.70	607.58
35.20	551.88	35.22	591.22	34.85	574.53	34.87	561.75	34.88	552.16	34.90	609.53
35.40	549.37	35.42	593.15	35.05	574.33	35.07	550.82	35.08	550.82	35.10	606.84
35.60	547.15	35.62	593.79	35.25	576.76	35.27	556.89	35.28	553.67	35.30	609.89
35.80	544.07	35.81	583.70	35.45	578.96	35.46	556.86	35.48	549.31	35.49	602.72
36.00	565.12	36.01	608.43	35.65	569.59	35.66	546.78	35.68	551.13	35.69	605.40
36.19	572.11	36.21	614.19	35.84	592.62	35.86	576.11	35.87	571.40	35.89	628.84
36.39	575.88	36.41	612.16	36.04	589.49	36.06	577.50	36.07	570.11	36.09	623.97
36.59	569.69	36.61	612.15								

TABLE IV.- AFTERBODY TEMPERATURES MEASURED ON PROJECT FIRE REENTRY PACKAGE - Concluded

Afterbody temperatures, °K											
$\phi = 120^\circ$				$\phi = 240^\circ$							
Time from 122 km (400 000 ft) sec	$\frac{x}{l} = .56$	Time from 122 km (400 000 ft) sec	$\frac{x}{l} = .70$	Time from 122 km (400 000 ft) sec	$\frac{x}{l} = .19$	Time from 122 km (400 000 ft) sec	$\frac{x}{l} = .38$	Time from 122 km (400 000 ft) sec	$\frac{x}{l} = .56$	Time from 122 km (400 000 ft) sec	$\frac{x}{l} = .70$
36.79	565.42	36.80	612.87	36.24	589.99	36.26	572.70	36.27	570.06	36.29	628.66
36.99	559.41	37.00	608.55	36.44	587.71	36.45	571.82	36.47	567.02	36.48	627.75
37.19	582.59	37.20	625.65	36.64	588.85	36.65	573.46	36.67	571.85	36.68	624.87
37.38	581.57	37.40	629.55	36.83	586.11	36.85	572.26	36.87	570.12	36.88	629.95
37.58	574.66	37.60	628.26	37.03	597.98	37.05	589.27	37.06	582.06	37.08	639.99
37.78	582.00	37.79	626.77	37.23	602.75	37.25	585.22	37.26	581.57	37.28	637.28
37.98	583.39	37.99	627.41	37.43	597.98	37.44	585.15	37.46	581.51	37.47	638.02
38.18	585.82	38.19	631.37	37.63	596.95	37.64	587.69	37.66	578.84	37.67	645.29
38.37	585.99	38.39	632.92	37.82	600.28	37.84	592.09	37.86	583.90	37.87	647.89
38.57	586.40	38.59	633.23	38.02	603.22	38.04	584.29	38.05	584.29	38.07	635.46
38.77	579.96	38.78	629.75	38.22	601.29	38.24	583.44	38.25	585.48	38.27	644.14
38.97	582.16	38.98	632.51	38.42	602.35	38.43	589.49	38.45	589.49	38.46	643.01
39.17	582.41	39.18	629.20	38.62	605.66	38.63	585.68	38.65	602.59	38.66	640.51
39.36	584.02	39.38	632.62	38.82	608.38	38.83	587.84	38.85	601.19	38.86	642.27
39.56	589.16	39.58	630.57	39.01	602.48	39.03	592.20	39.04	586.03	39.06	638.46
39.76	584.89	39.78	627.93	39.21	602.12	39.23	581.92	39.24	586.09	39.26	640.37
39.96	576.14	39.97	619.13	39.41	603.98	39.42	588.13	39.44	589.16	39.46	645.40
40.16	574.78	40.17	624.64	39.61	601.48	39.62	568.97	39.64	580.67	39.65	634.67
40.35	570.78	40.37	613.01	39.81	588.33	39.82	571.32	39.84	580.96	39.85	631.14
40.55	559.89	40.57	610.14	40.00	585.45	40.02	574.24	40.03	574.24	40.05	628.82
40.75	577.84	40.77	626.89	40.20	589.03	40.22	566.99	40.23	568.07	40.25	628.58
40.95	582.40	40.96	631.71	40.40	547.42	40.42	562.06	40.43	565.31	40.45	617.01
41.15	581.52	41.16	627.43	40.60	604.98	40.61	578.36	40.63	580.45	40.64	635.04
41.34	580.61	41.36	623.16	40.80	598.50	40.81	585.01	40.83	585.53	40.84	640.01
41.54	570.78	41.56	614.95	40.99	592.51	41.01	575.11	41.02	583.65	41.04	624.30
41.74	561.11	41.76	611.15	41.19	599.04	41.21	578.46	41.22	580.07	41.24	635.75
41.94	594.93	41.95	626.92	41.39	588.85	41.41	571.85	41.42	579.89	41.44	625.40
42.14	590.71	42.15	634.53	41.59	584.83	41.60	575.69	41.62	568.67	41.63	627.47
42.33	587.75	42.35	634.80	41.79	610.67	41.80	600.00	41.82	601.02	41.83	652.32
42.53	585.29	42.55	633.48	41.98	608.04	42.00	593.77	42.01	597.85	42.03	643.70
42.73	587.20	42.75	627.75	42.18	611.27	42.20	594.91	42.21	594.91	42.23	648.10
42.93	583.16	42.94	630.58	42.38	607.33	42.40	590.42	42.41	598.11	42.43	606.31
43.13	583.87	43.14	629.52	42.58	600.03	42.59	593.36	42.61	590.28	42.62	639.04
43.33	584.41	43.34	628.95	42.78	606.35	42.79	588.32	42.81	591.92	42.82	637.79
43.52	580.58	43.54	623.78	42.97	600.80	42.99	584.39	43.01	587.98	43.02	628.49
43.72	559.84	43.74	597.98	43.17	597.72	43.19	585.95	43.20	648.91	43.22	636.12
				43.37	603.24	43.39	593.48	43.40	583.73	43.42	632.00
				43.57	602.61	43.58	586.15	43.60	590.27	43.61	618.55

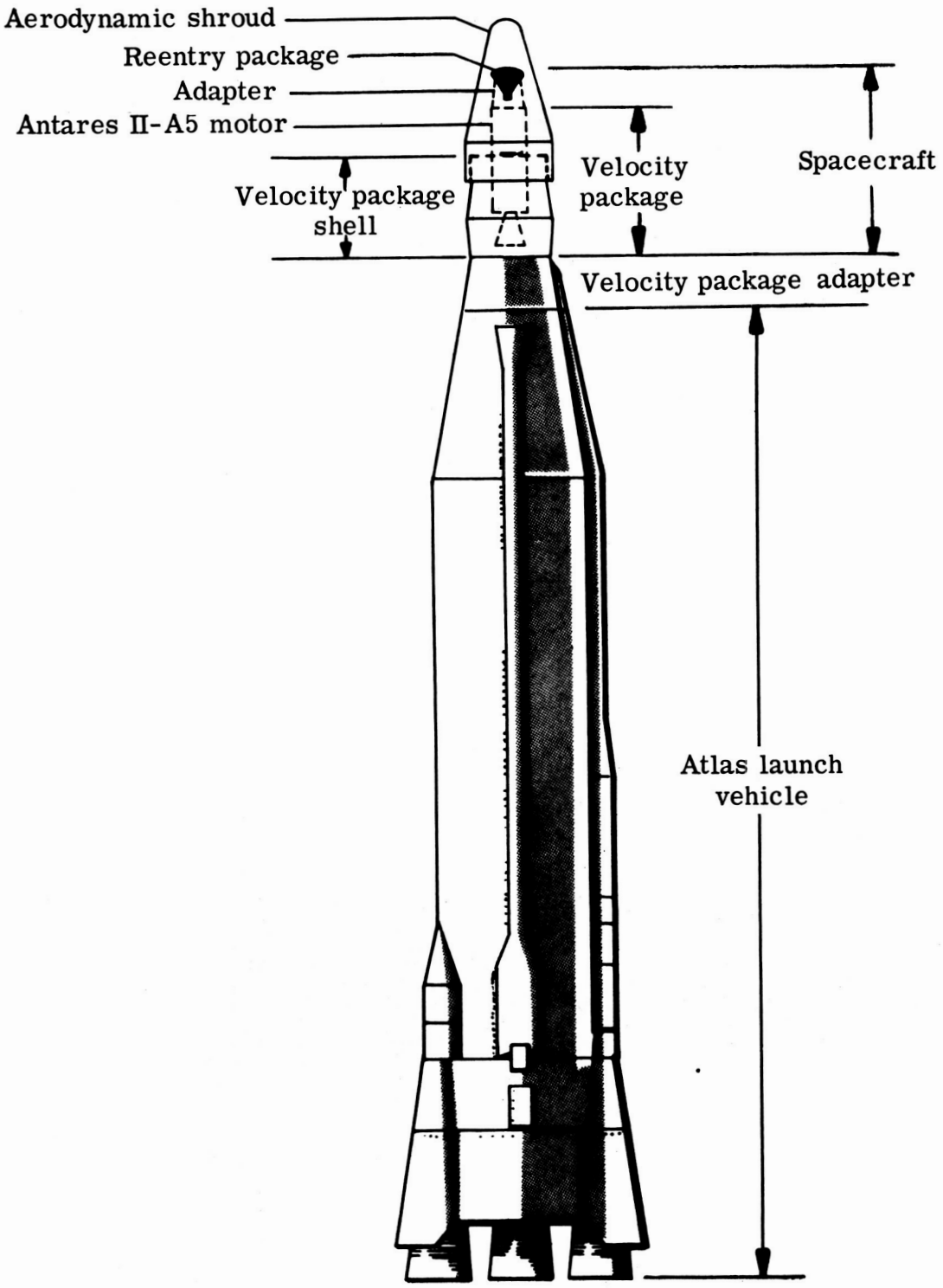

Figure 1.- Schematic drawing of Project Fire space vehicle.

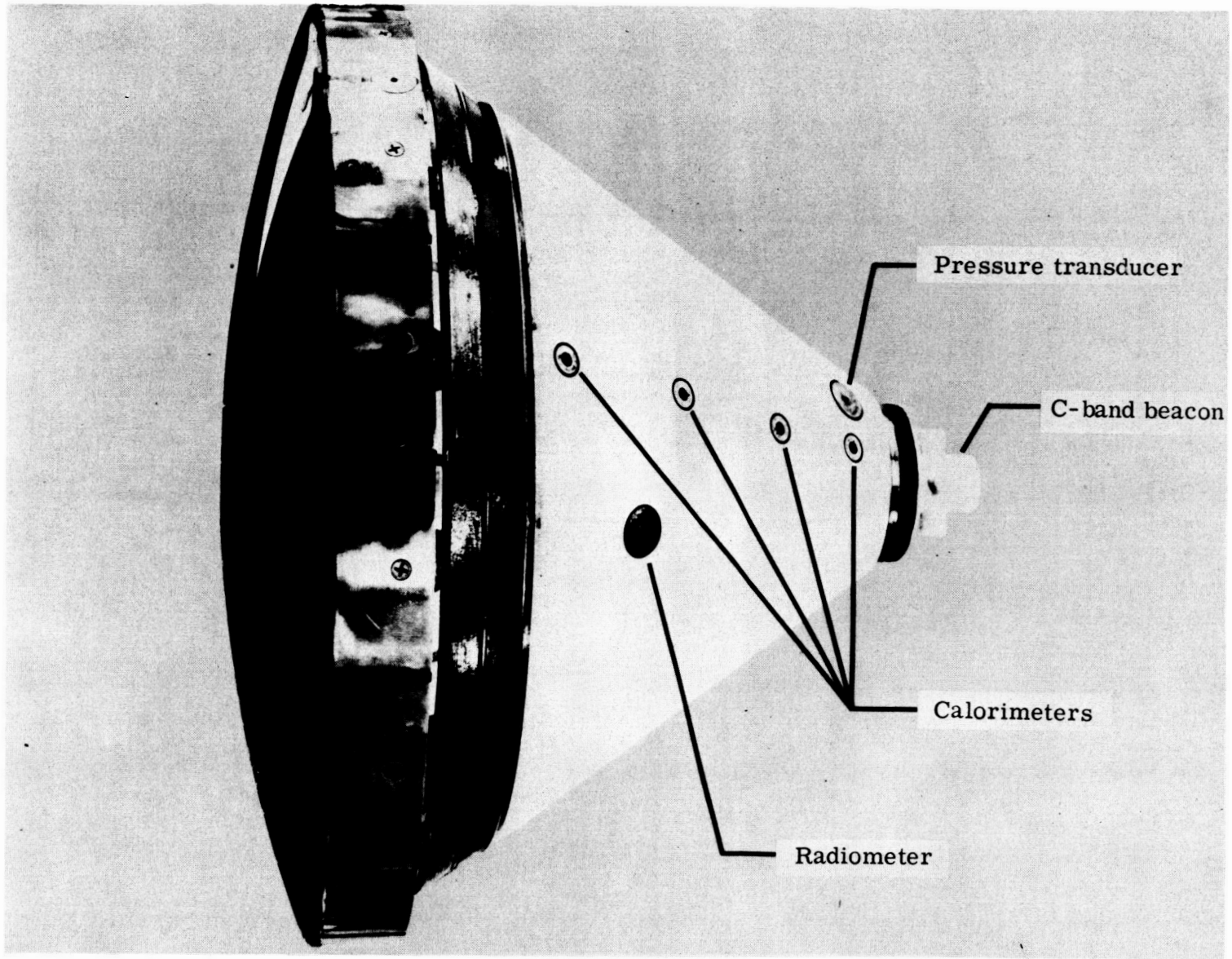

Figure 2.- Photograph of reentry package.

L-66-4594

Beryllium heat-shield number	D_m		R_n		R_c	
	cm	in.	cm	in.	cm	in.
1	67.15	26.44	93.47	36.80	1.01	0.40
2	62.99	24.80	80.51	31.70	3.55	1.40
3	58.79	23.11	70.20	27.64	.609	.24

Key to afterbody instrumentation

+ - Gold calorimeters
△ - Pressure sensor
○ - Radiometer
▨ - Telemetry antenna
▪ - C-band beacon antenna

NOTE: Dimensional location of afterbody sensors is shown in Table I.

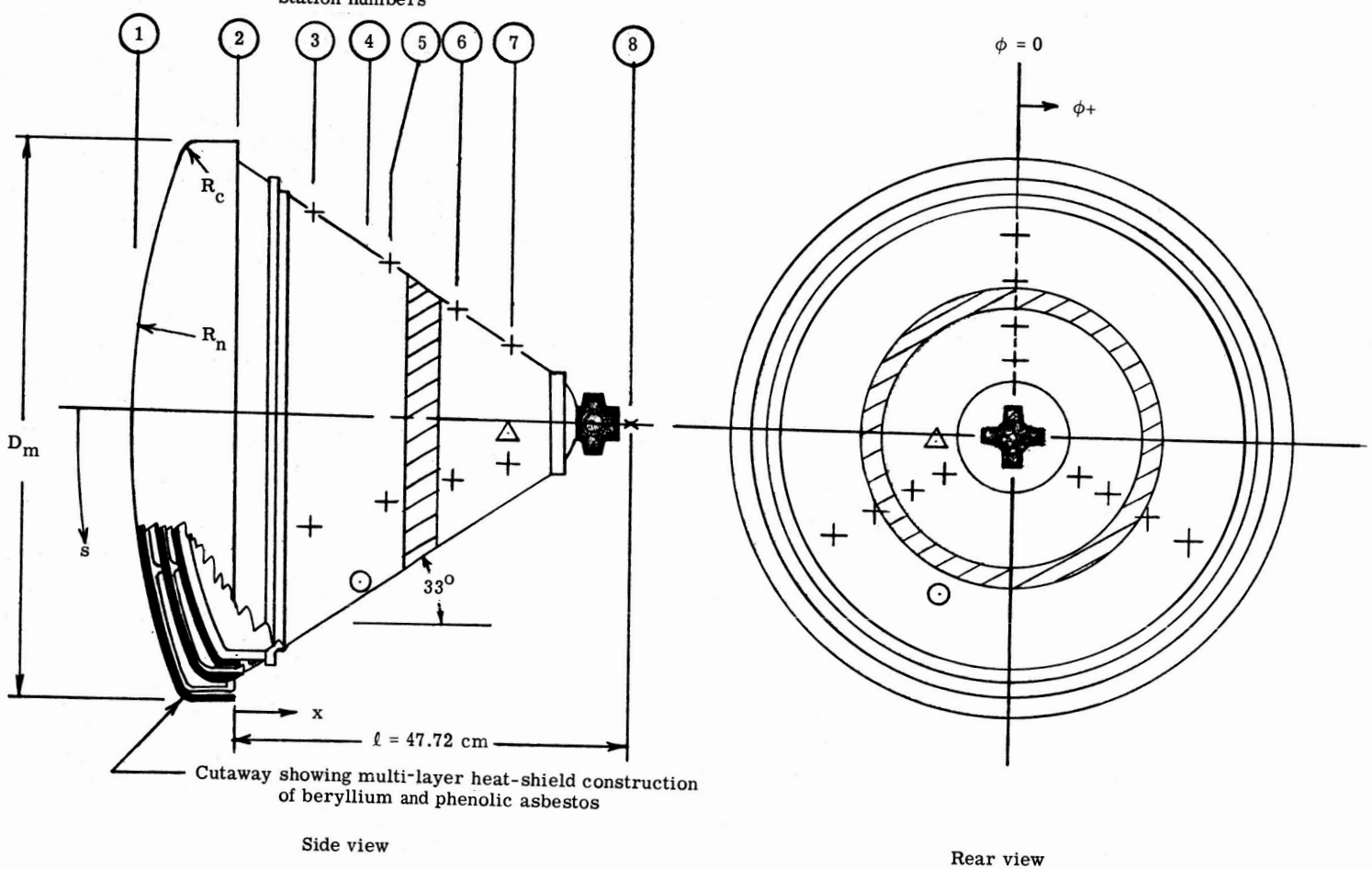

Figure 3.- Reentry package geometry.

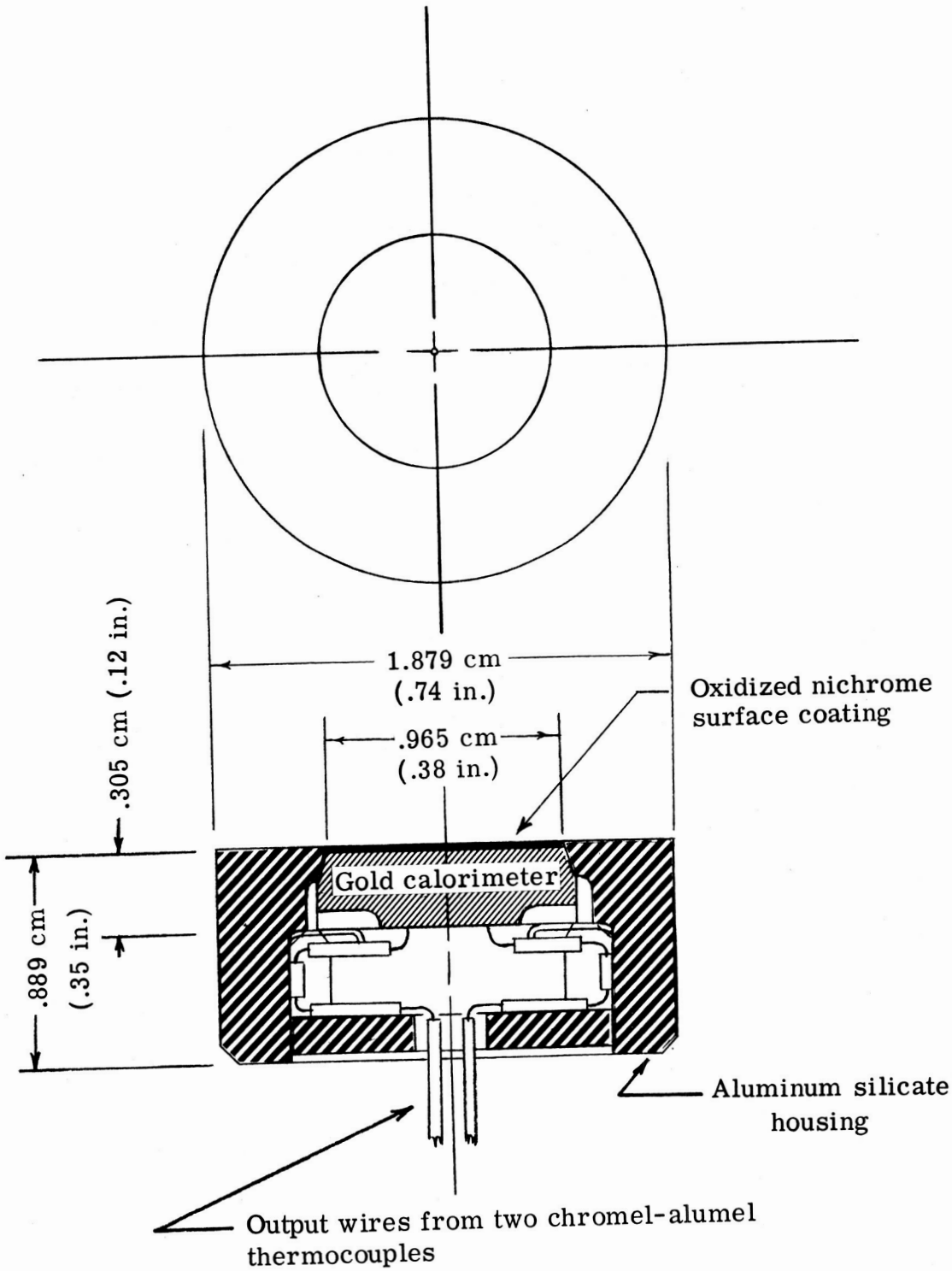

Figure 4.- Schematic drawing of gold calorimeter and insulating housing.

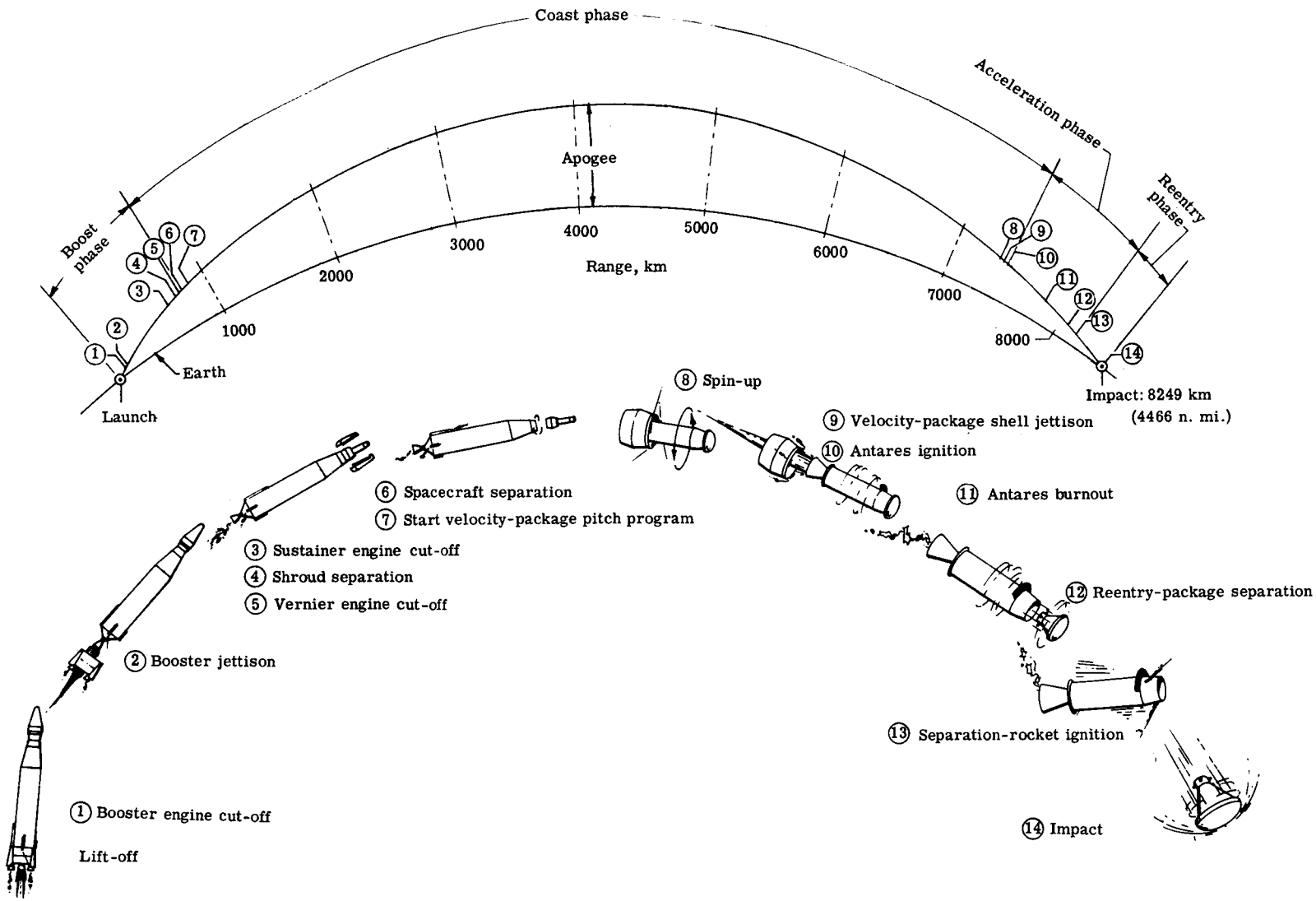

Figure 5.- Sequence of events in Project Fire flight II.

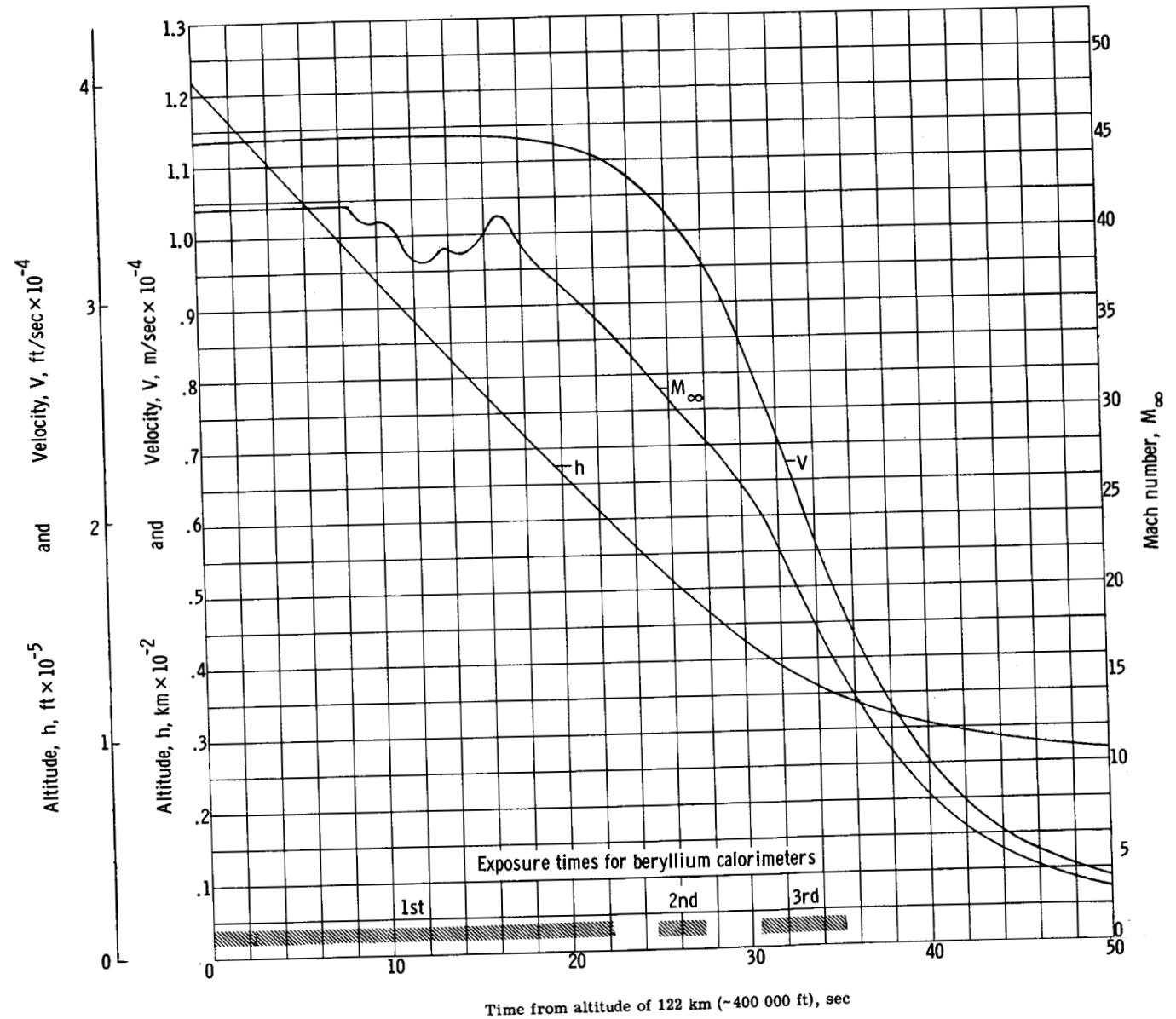

Figure 6.- Reentry trajectory parameters.

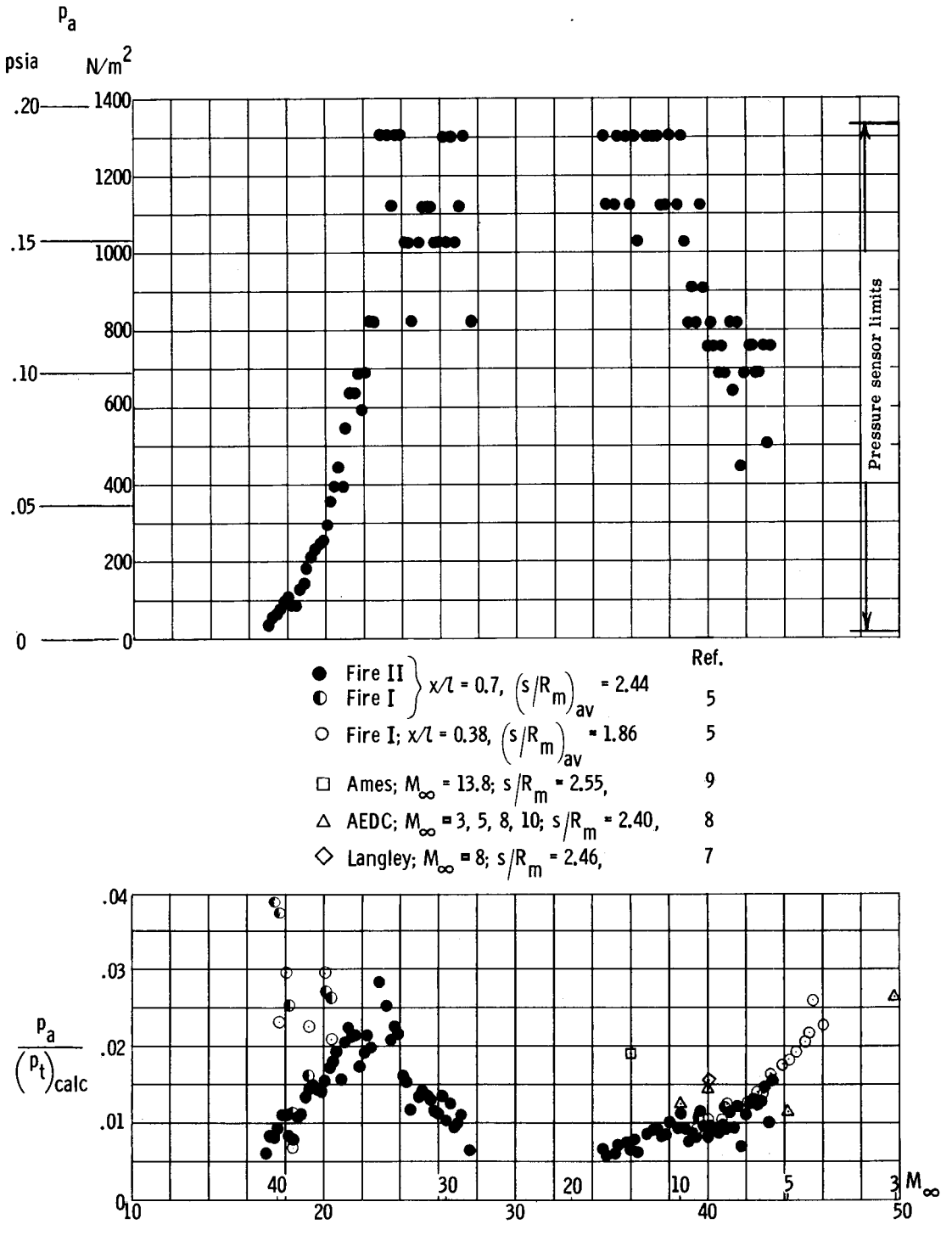

Figure 7.- Project Fire afterbody pressure measurements.

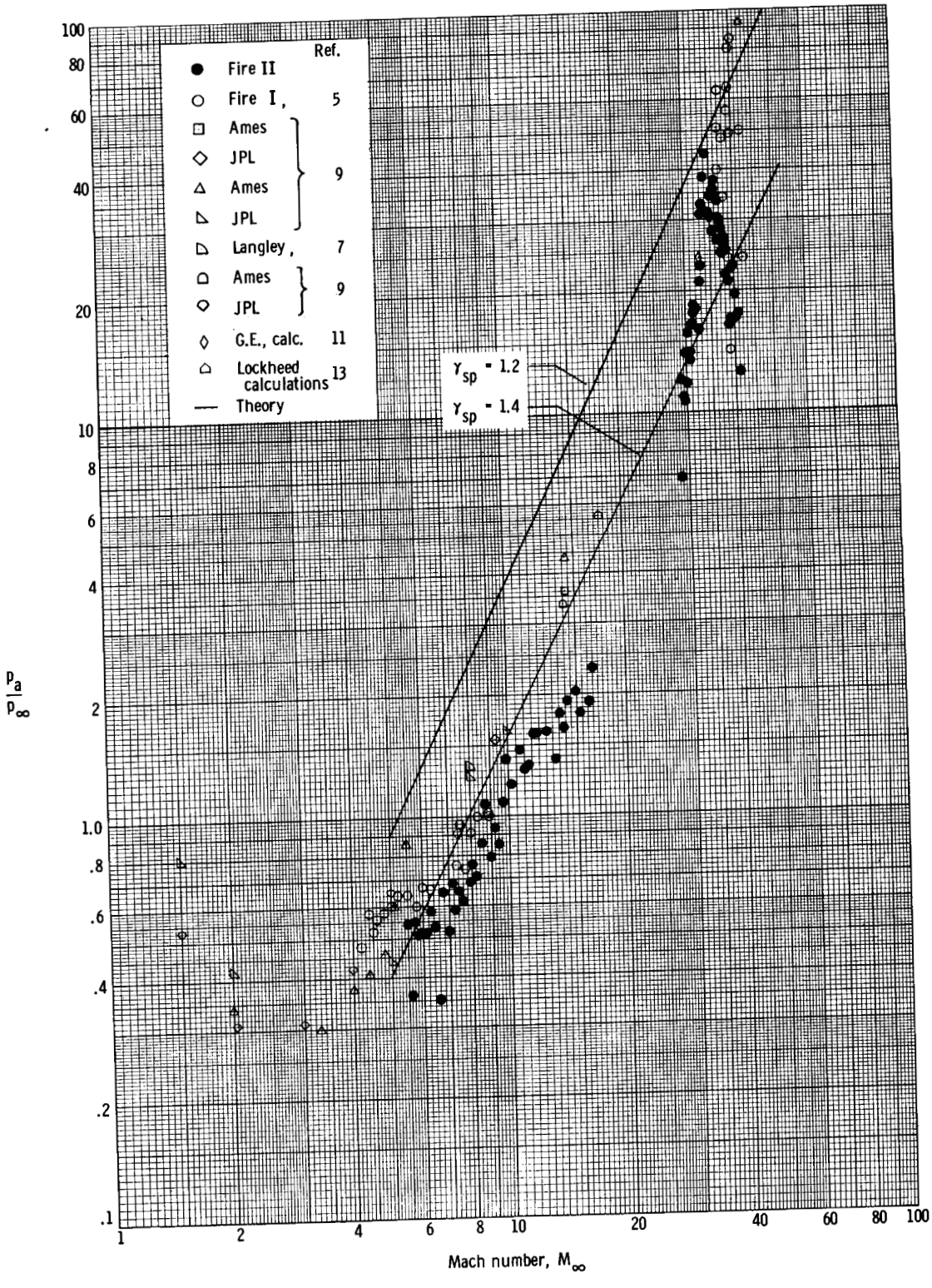

Figure 8.- Correlation of flight and ground-facility measurements of afterbody pressures on Apollo shape bodies.

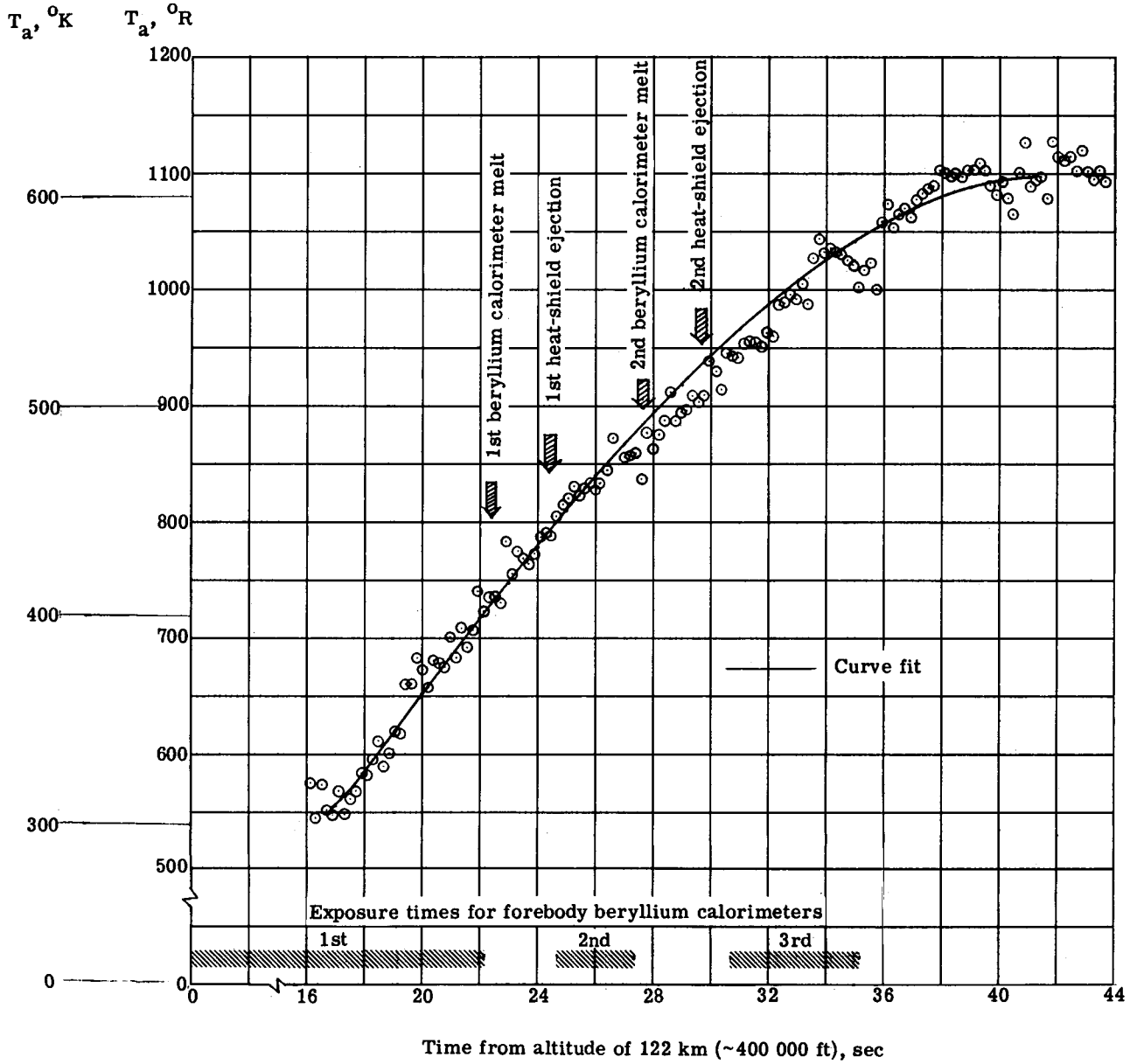

(a) $\Phi = 0^0$; $x/l = 0.19$.

Figure 9.- Variation of afterbody temperature with time from an altitude of 122 km (≈400 000 ft).

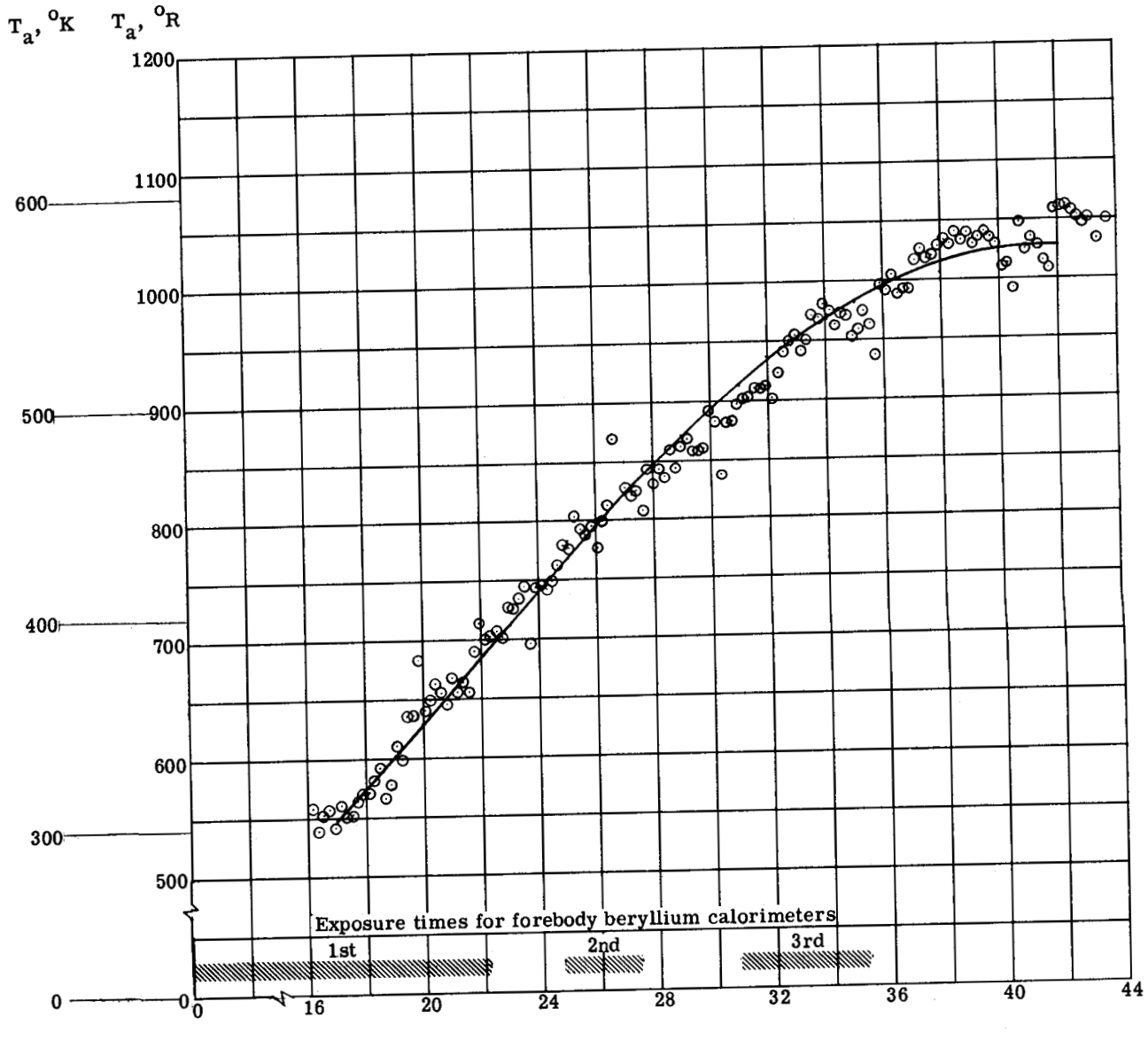

(b) $\Phi = 0^0$; $x/l = 0.38$.

Figure 9.- Continued.

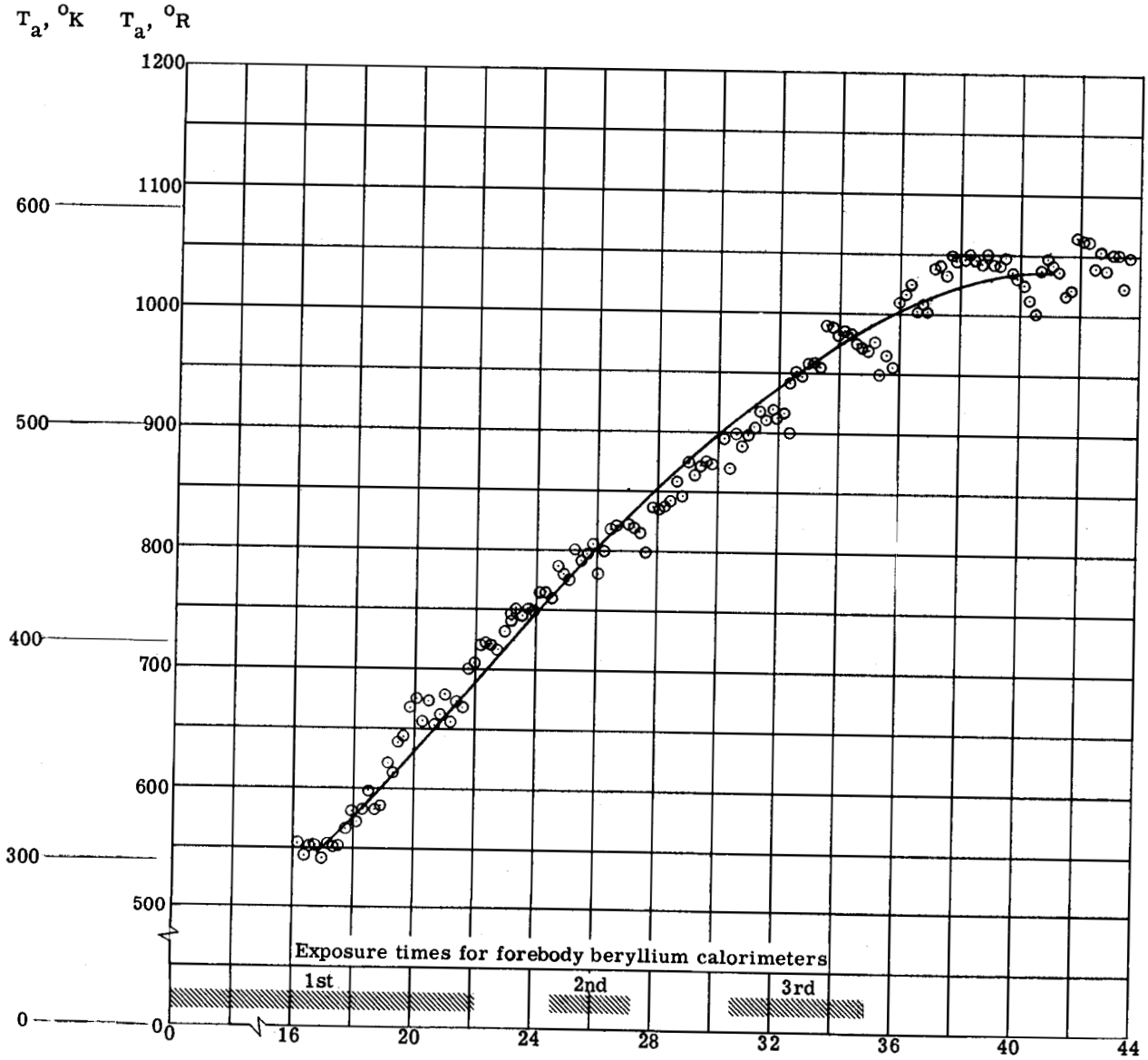

(c) $\Phi = 0^0$; $x/l = 0.56$.

Figure 9.- Continued.

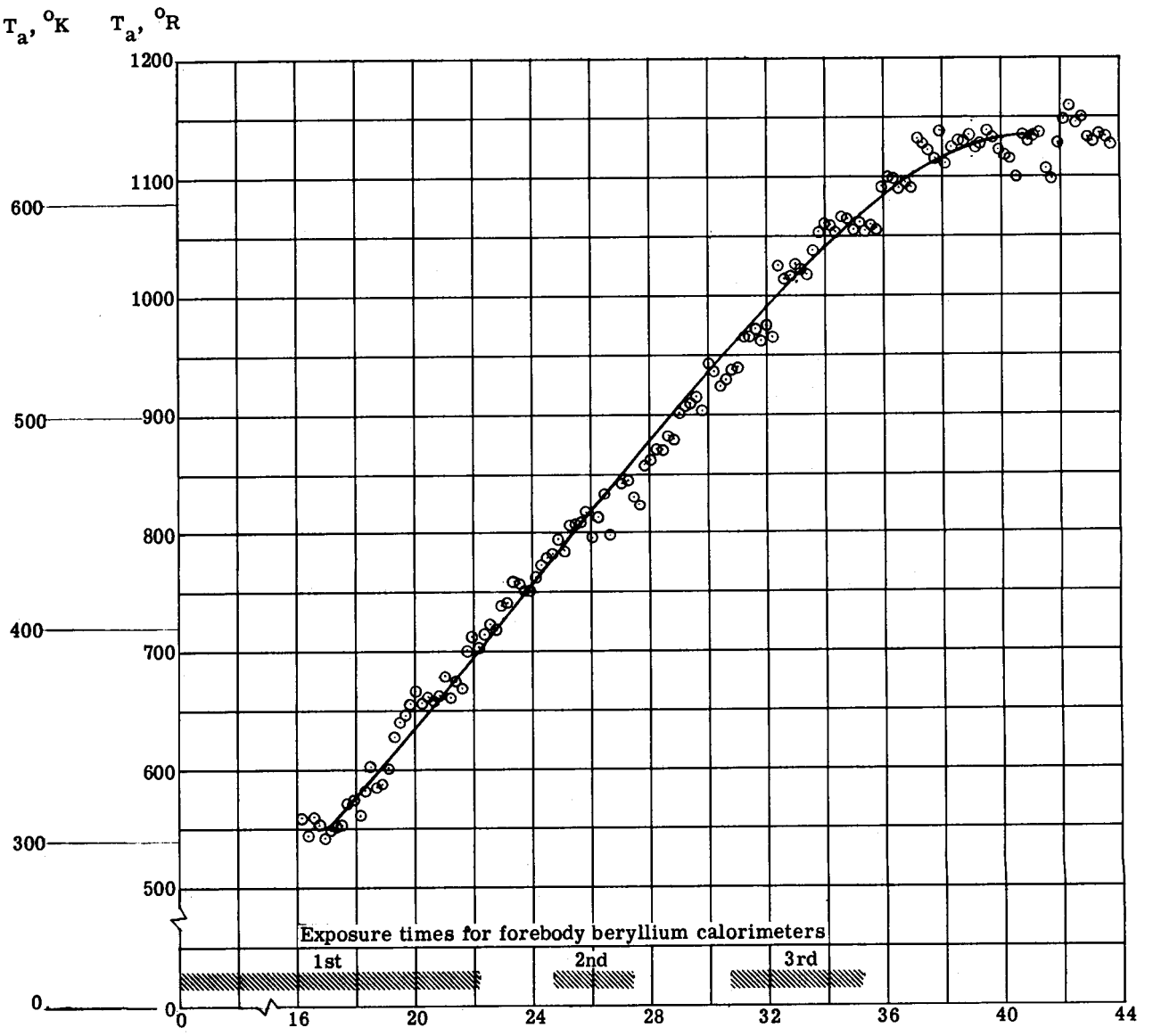

(d) $\Phi = 0^0$; $x/l = 0.70$.

Figure 9.- Continued.

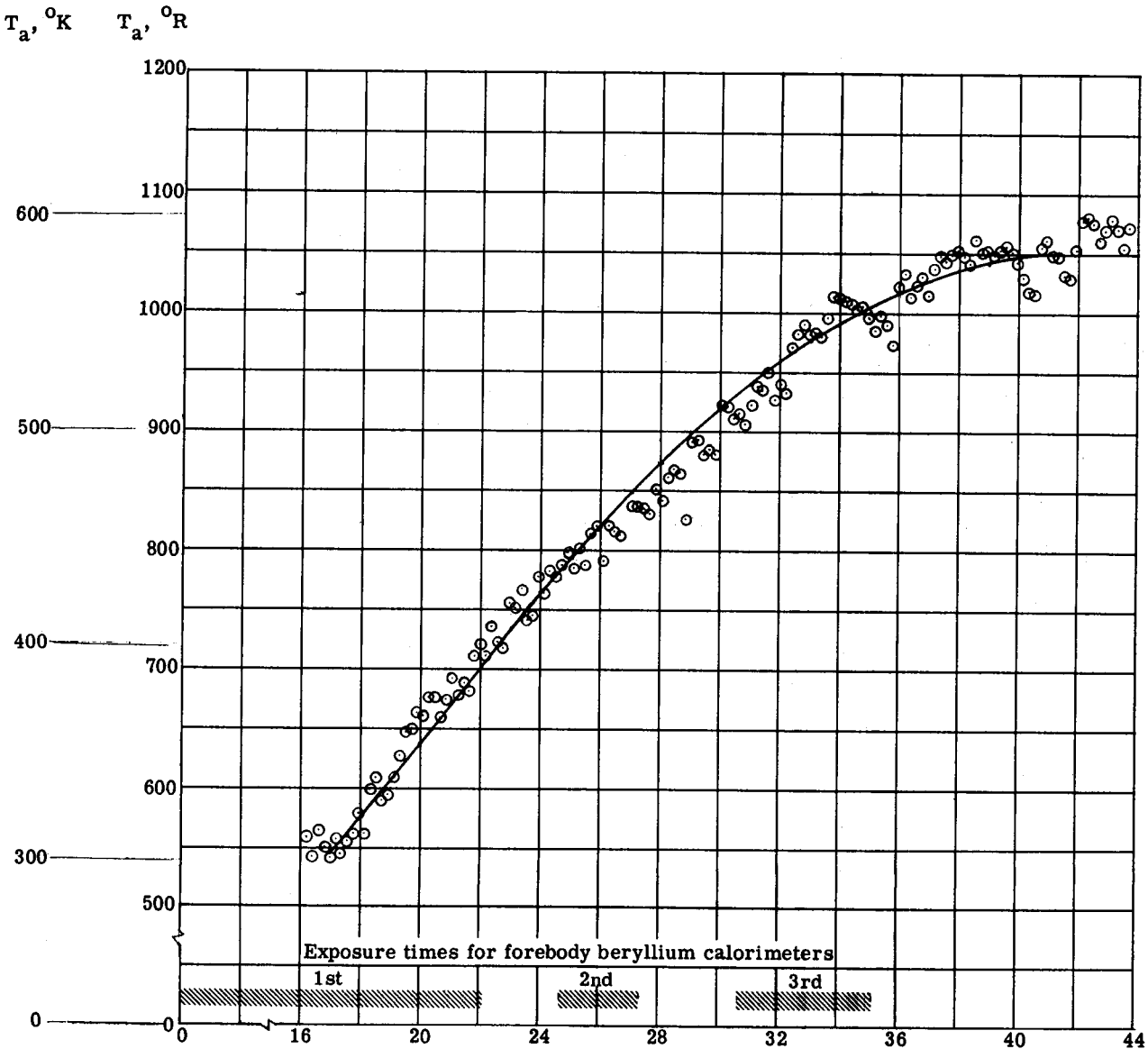

(e) $\Phi = 120^0$; $x/l = 0.19$.

Figure 9.- Continued.

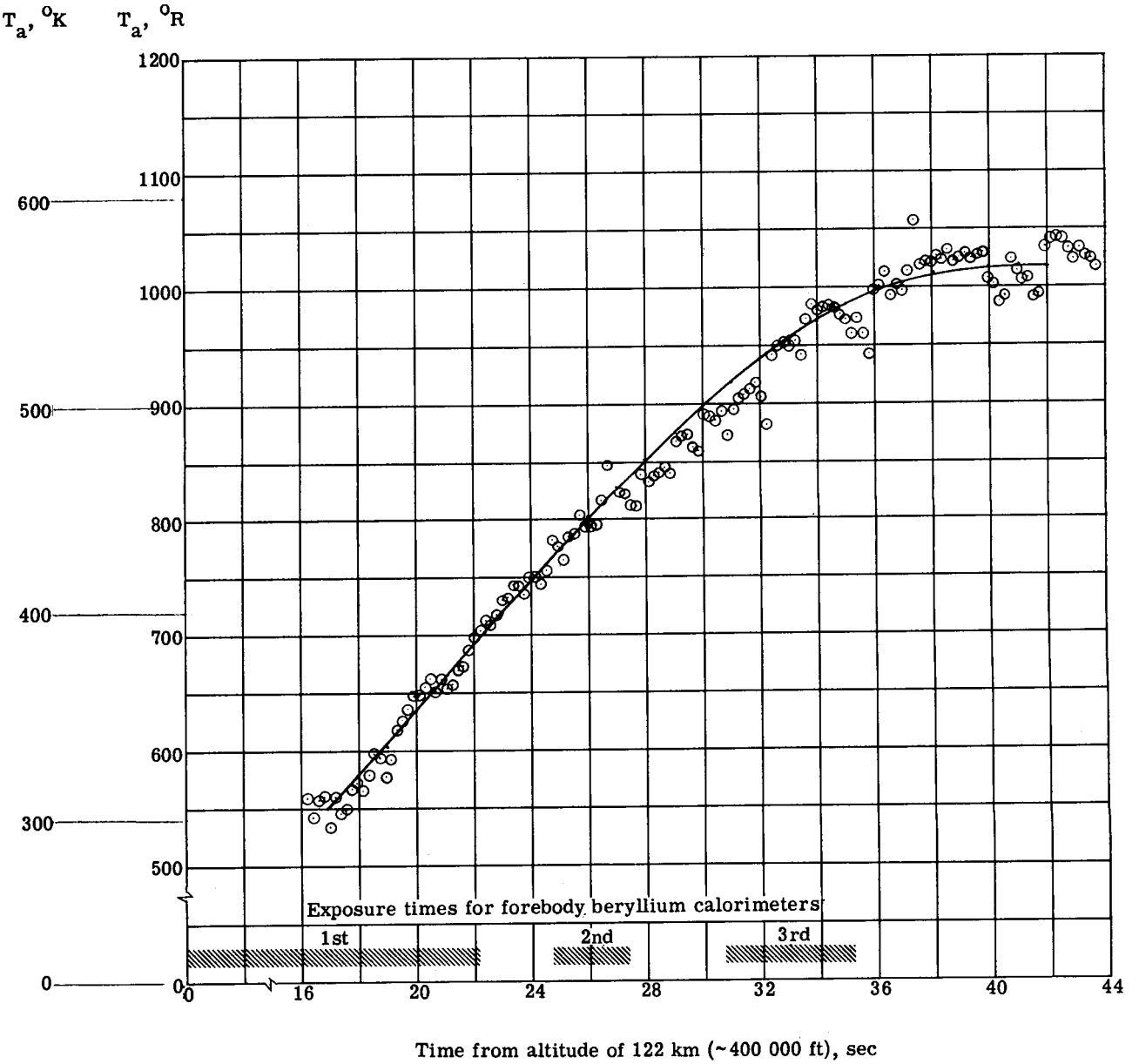

(f) $\Phi = 120^{\circ}$; $x/l = 0.38$.

Figure 9.- Continued.

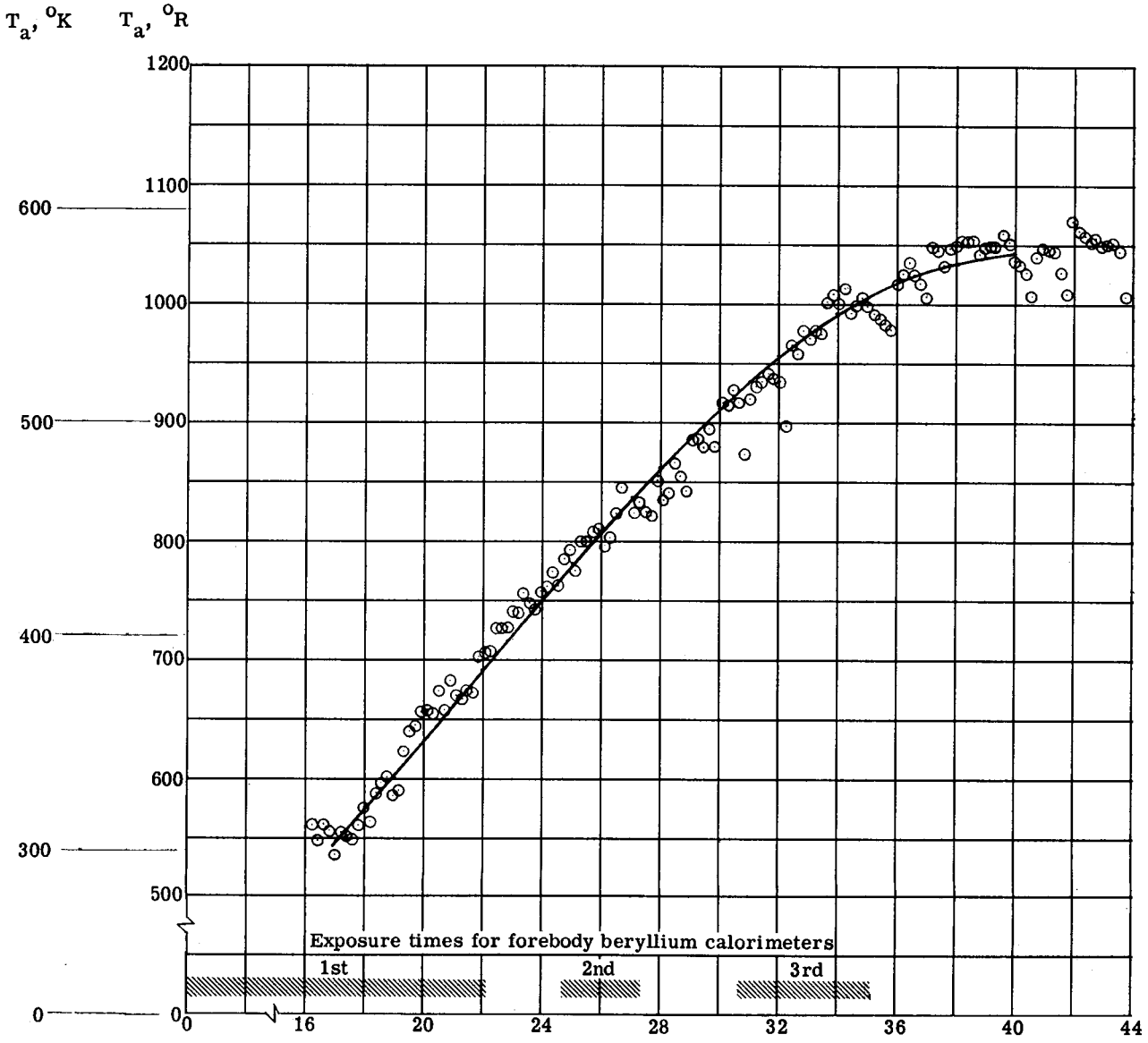

(g) $\Phi = 120^0$; $x/l = 0.56$.

Figure 9.- Continued.

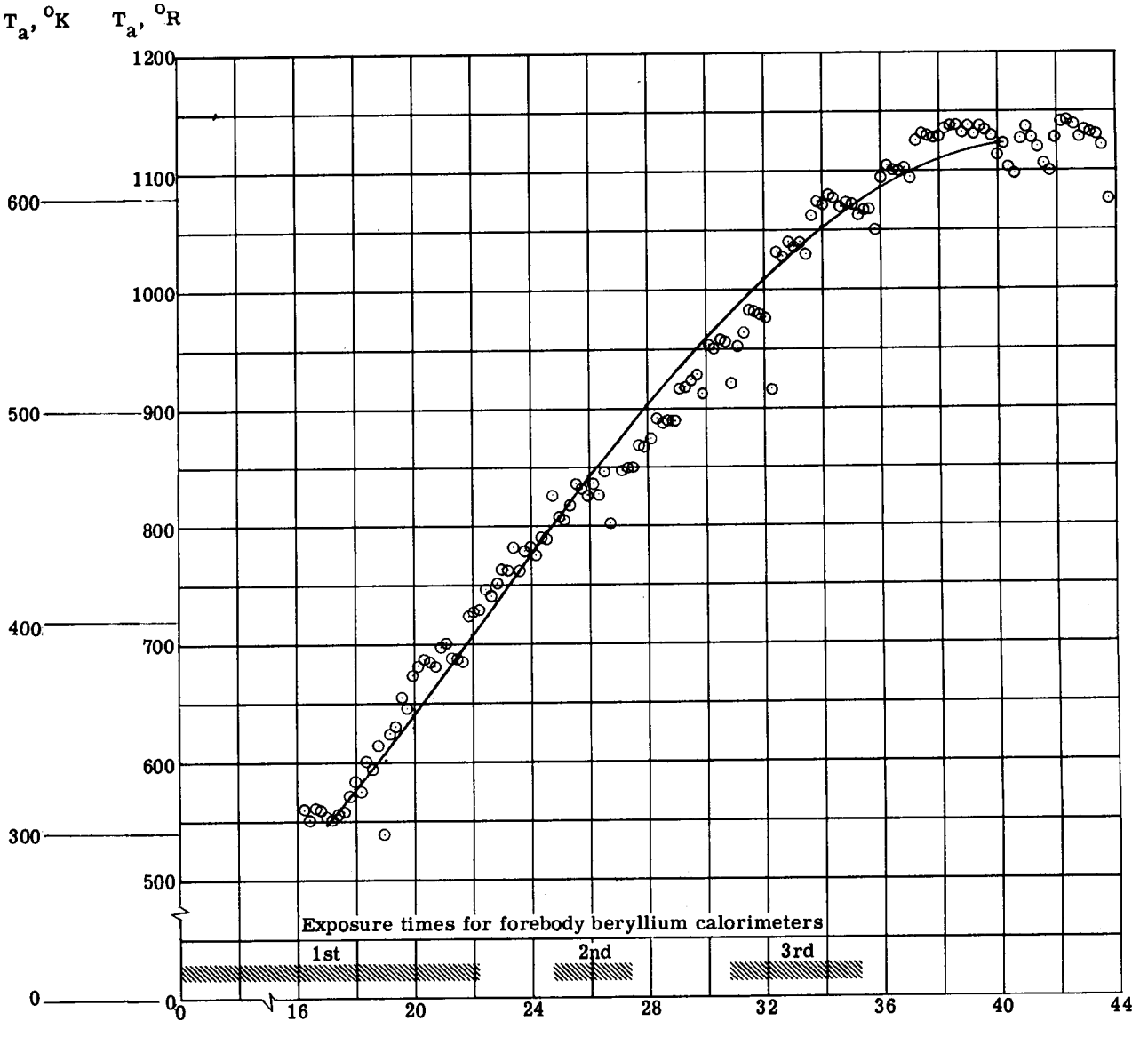

(h) $\Phi = 120^0$; $x/l = 0.70$.

Figure 9.- Continued.

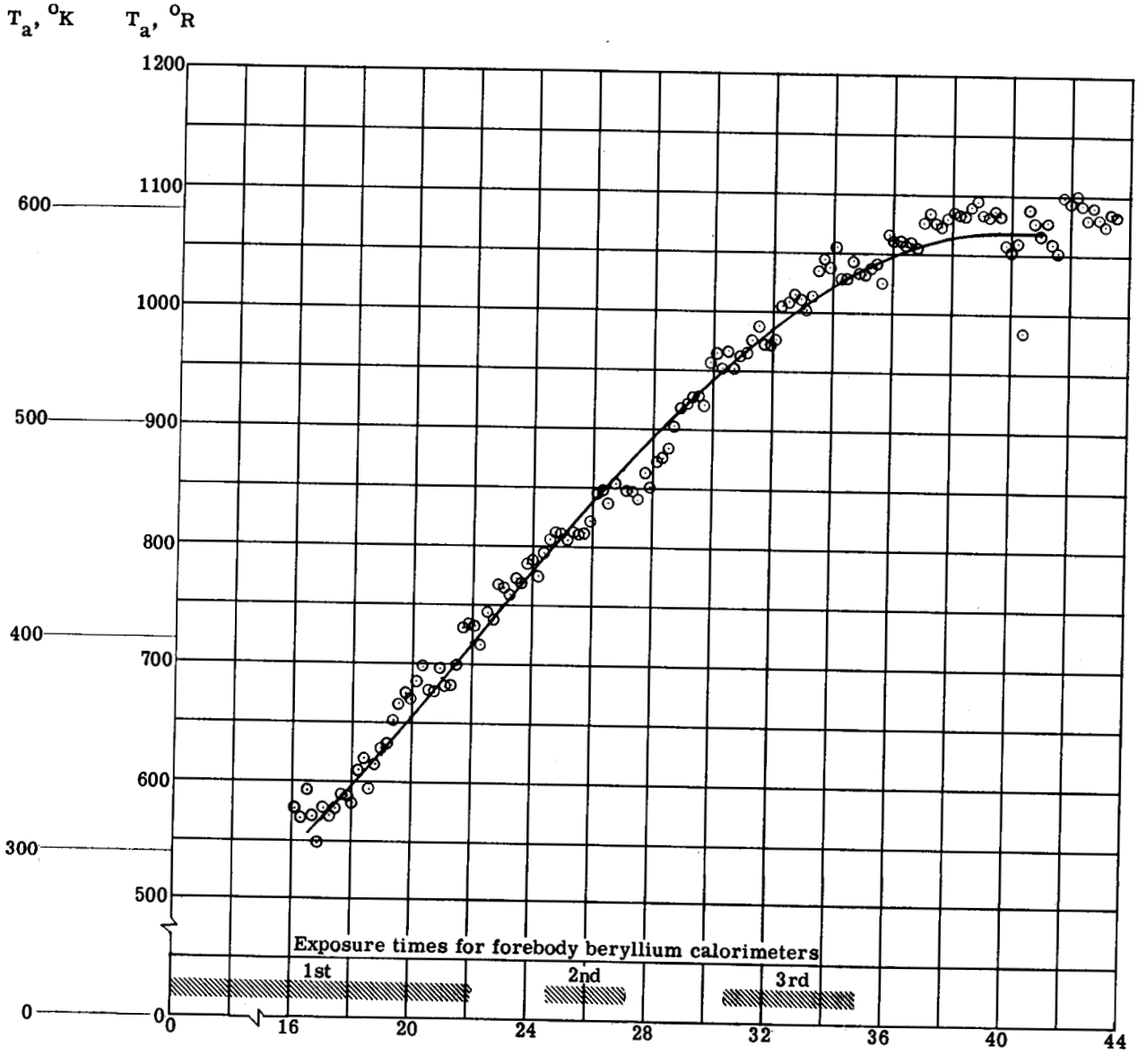

(i) $\Phi = 240^0$; $x/l = 0.19$.

Figure 9.- Continued.

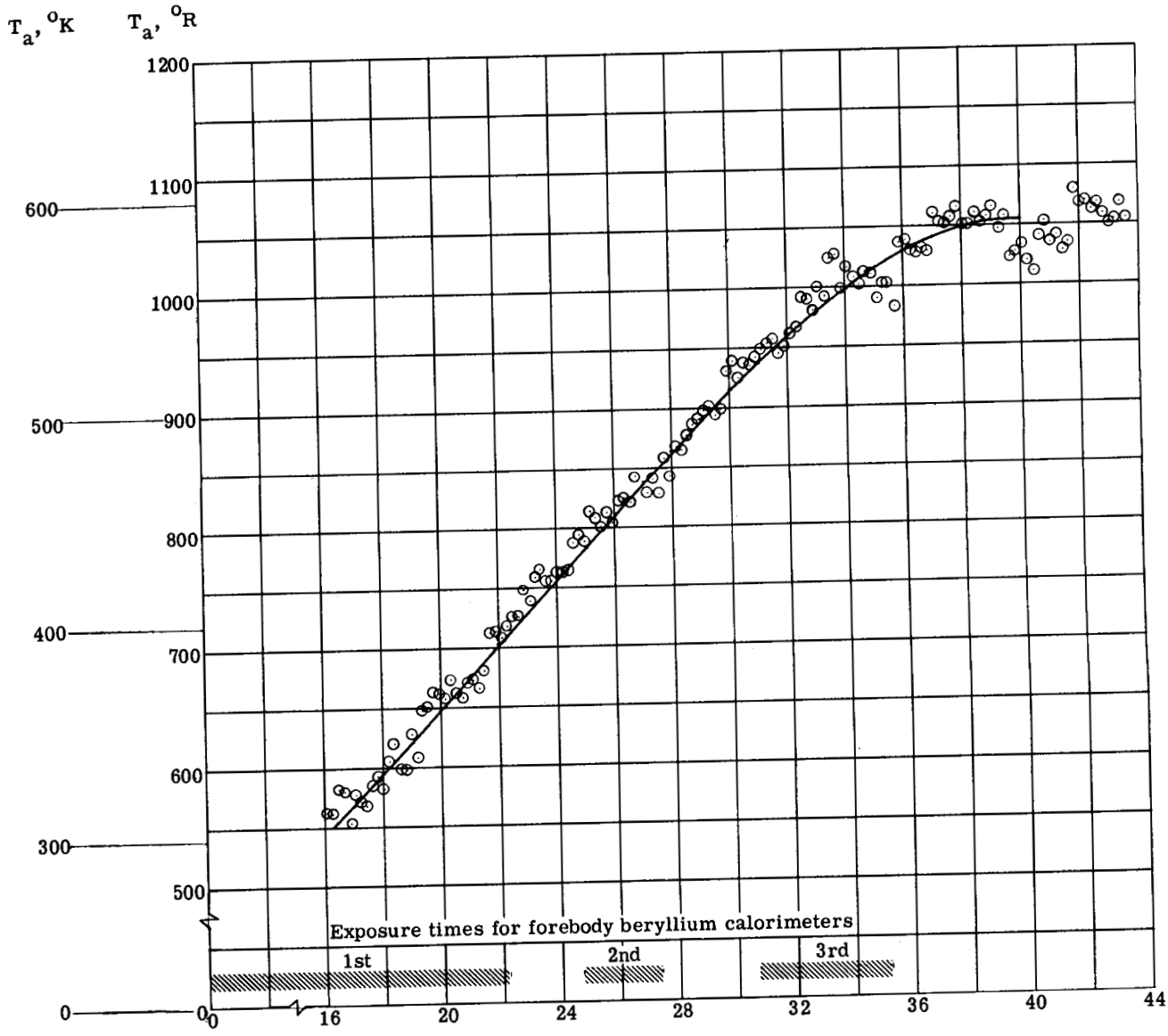

(j) $\Phi = 240^0$; $x/l = 0.38$.

Figure 9.- Continued.

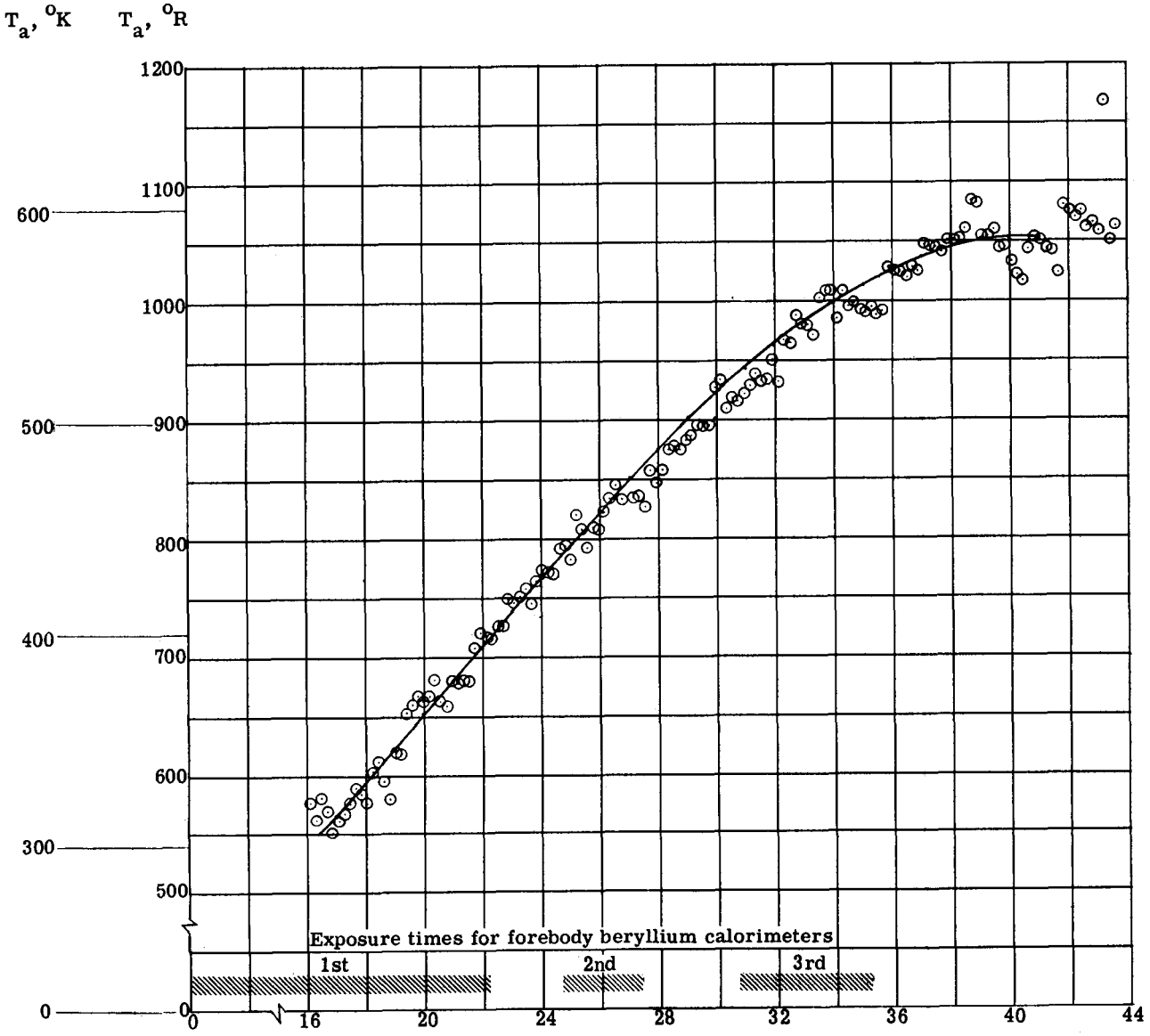

(k) $\Phi = 240^0$; $x/l = 0.56$.

Figure 9.- Continued.

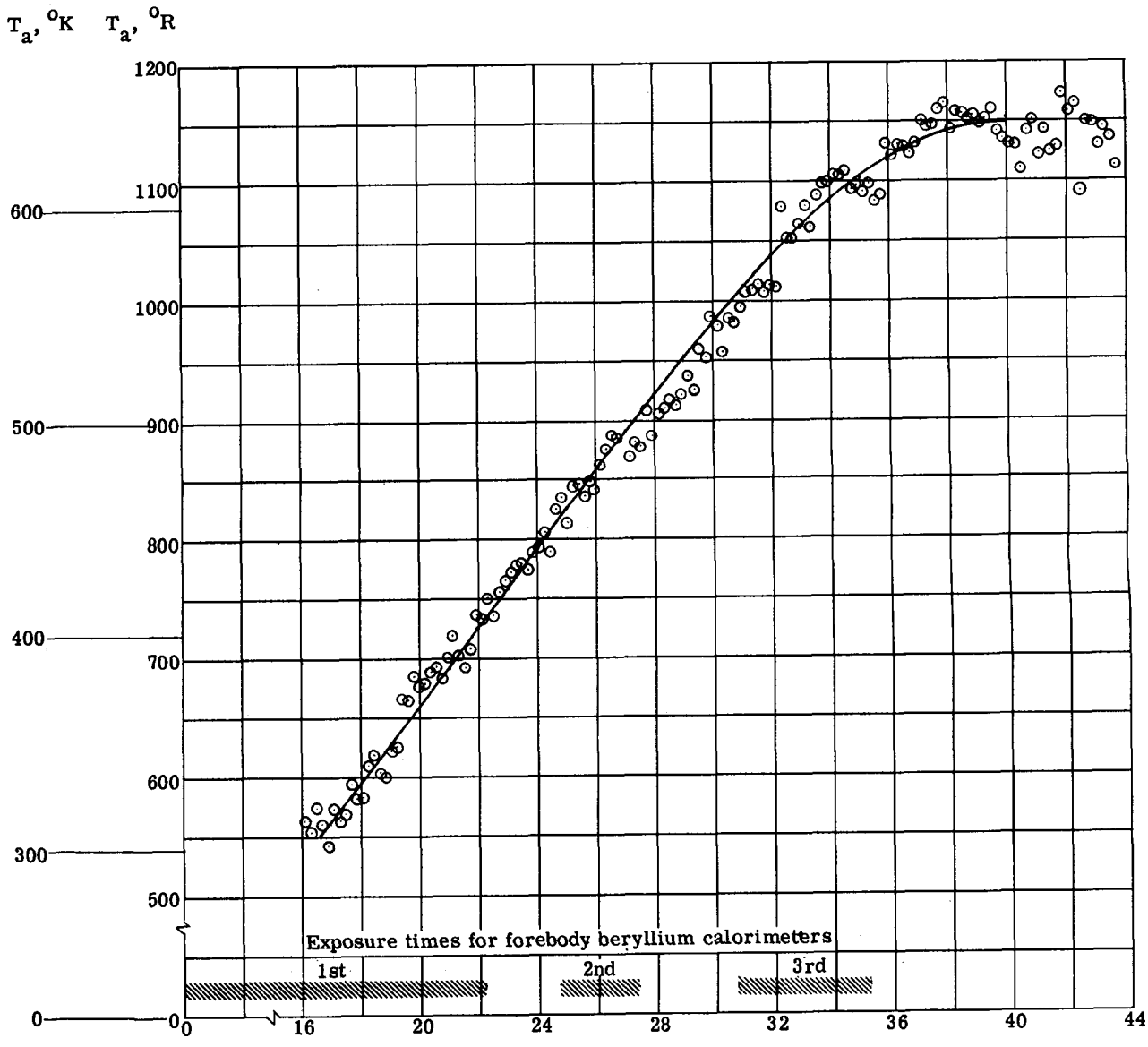

(l) $\Phi = 240^0$; $x/l = 0.70$.

Figure 9.- Concluded.

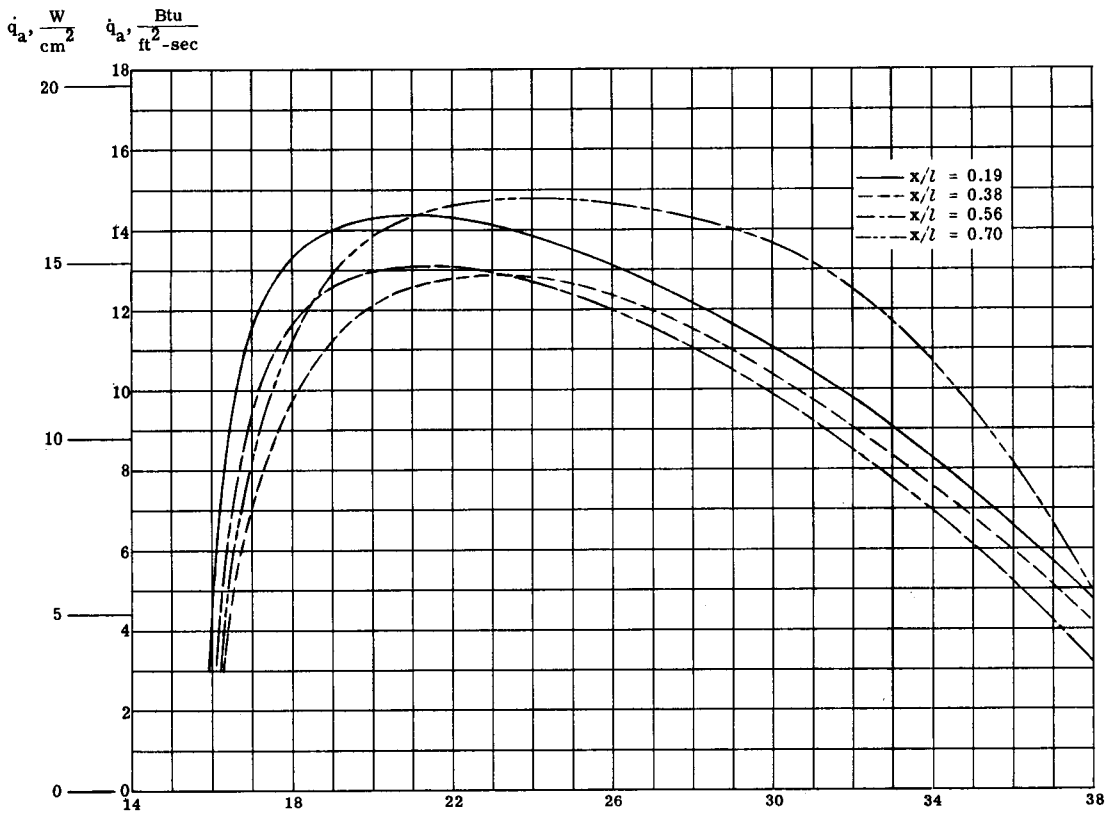

(a) $\Phi = 0^0$.

Figure 10.- Variation of afterbody heating rates with time from altitude of 122 km (≈400 000 ft).

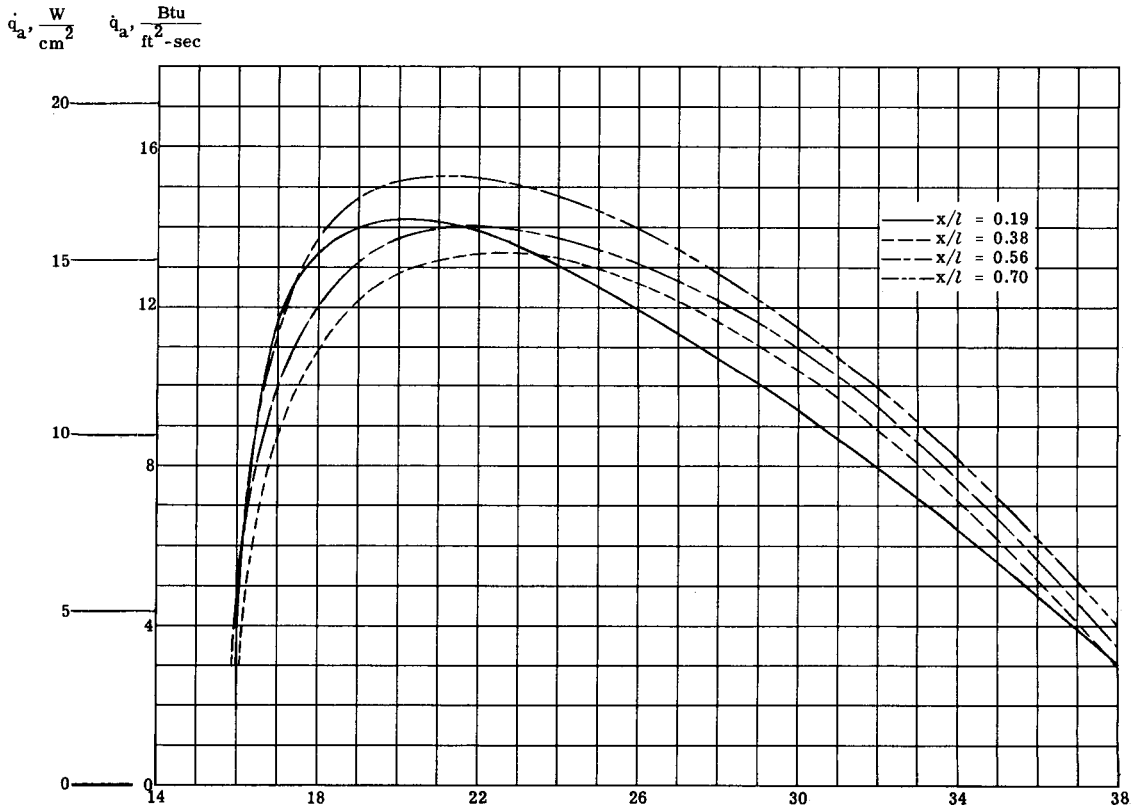

(b) $\Phi = 120^{\circ}$.

Figure 10.- Continued.

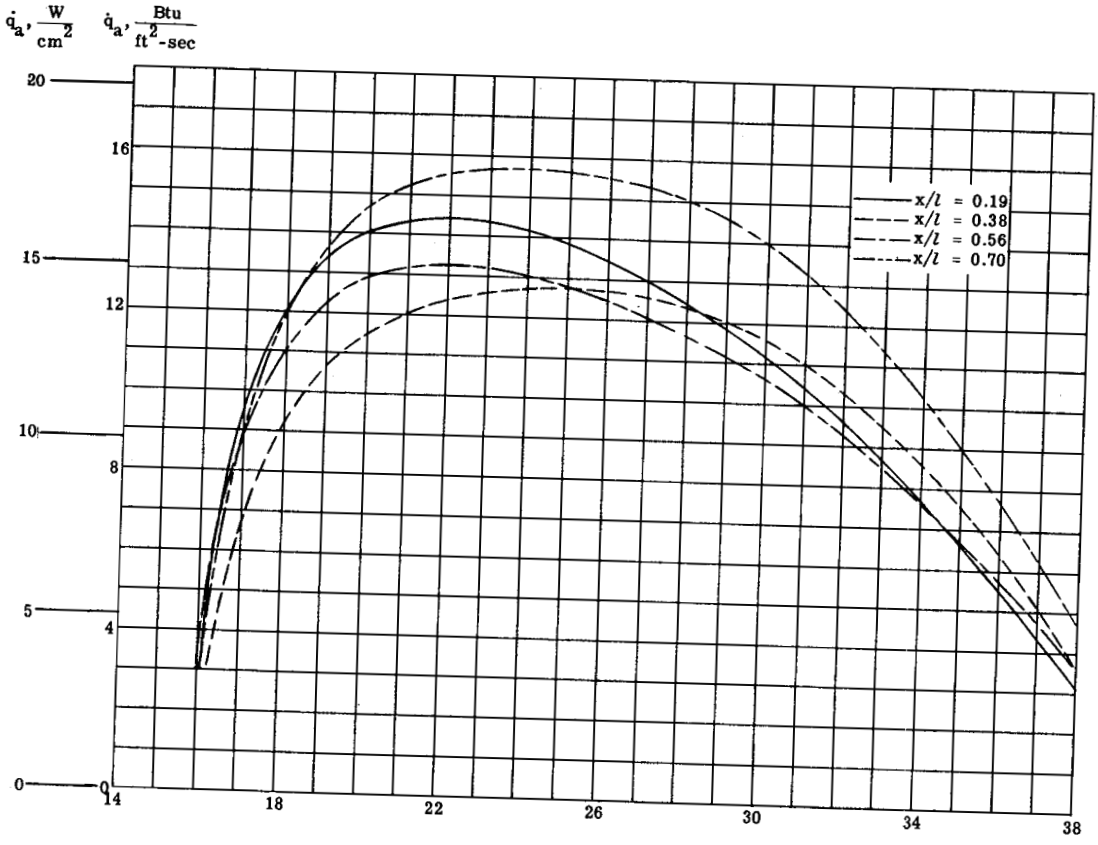

(c) $\Phi = 240^0$.

Figure 10.- Concluded.

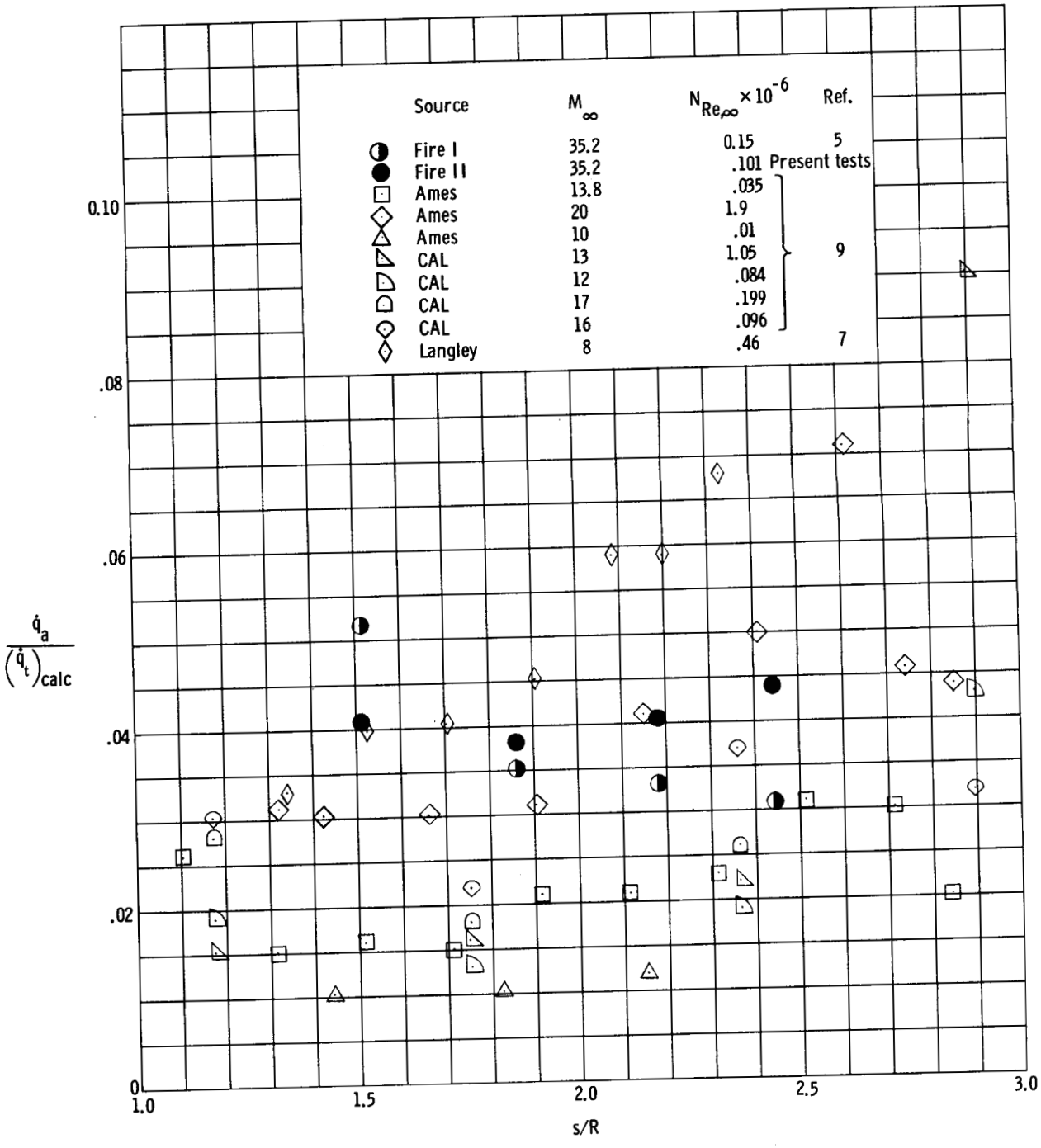

Figure 11.- Effect of longitudinal location on afterbody heating rates.

NASA-Langley, 1966 L-4897